MATERIALS PHYSICS AND MECHANICS REVIEW

Submitted: August 19, 2025 **Revised: September 8, 2025** **Accepted: September 25, 2025**

Micromechanics of misfit stress relaxation in heterogeneous crystalline nanostructures: a review

M.Yu. Gutkin [1–3]✉, A.L. Kolesnikova [1,2], S.A. Krasnitckii [2], K.N. Mikaelyan [1], D.A. Petrov [1], A.E. Romanov [2,4], A.M. Smirnov [2]

[1] Institute for Problems in Mechanical Engineering, Russian Academy of Sciences, St. Petersburg, Russia

[2] ITMO University, St. Petersburg, Russia

[3] Peter the Great St. Petersburg Polytechnic University, St. Petersburg, Russia

[4] Ioffe Institute, St. Petersburg, Russia

✉ m.y.gutkin@gmail.com

ABSTRACT

Theoretical models of misfit stress relaxation in heterogeneous crystalline nanostructures are reviewed in brief. It is shown that the main channel of relaxation is the formation of misfit dislocations. Some mathematical tools for continuum modeling of misfit stress relaxation through generation of discrete dislocations in spherical and cylindrical nanostructures are considered with special attention to the strain energies of the dislocations and the energies of elastic interaction between them. The critical conditions and energy barriers for the formation of prismatic dislocation loops and straight edge misfit dislocations in core-shell nanoparticles and nanowires with various types of cores, in Janus nanoparticles and nanowires, in axially inhomogeneous nanowires with transverse interfaces, and in free-standing composite nanolayers are discussed.

KEYWORDS

misfit stress • heterogeneous nanostructures • stress relaxation • misfit dislocations • Janus nanoparticles Janus nanowires • free-standing composite nanolayers • dislocation loops core-shell nanoparticles core-shell nanowires

Funding. *The authors are thankful to the Ministry of Education and Science of the Russian Federation for support under the state assignment No. 124041100008-5 for the Institute for Problems in Mechanical Engineering of the Russian Academy of Sciences.*

Citation: Gutkin MYu, Kolesnikova AL, Krasnitckii SA, Mikaelyan KN, Petrov DA, Romanov AE, Smirnov AM. Micromechanics of misfit stress relaxation in heterogeneous crystalline nanostructures: a review. *Materials Physics and Mechanics*. 2025;53(5): 1–34.
http://dx.doi.org/10.18149/MPM.5352025_1

Introduction

Heterogeneous crystalline nanostructures serve as the basis of modern devices in nano- and microelectronics, optoelectronics, photonics, etc. It is well known that their physical properties and performance characteristics strongly depend on elastic misfit strains caused by differences in crystal lattice parameters. Under certain conditions, the misfit strains and stresses relax through the formation of various defects [1–5], which can lead to a significant deterioration in the properties of nanostructures. The most common way of such relaxation is the formation of misfit dislocations (MDs) at the interfaces. Theoretical and experimental studies of relaxation processes with the formation of MDs

have been carried out since the mid-twentieth century (see, for example, some earlier papers [6,7] and more recent books [8–13] and reviews [14–27]). However, the discussion of the sources, mechanisms, and critical conditions for the appearance of MDs in real inhomogeneous crystalline nanostructures is still of great interest [25–27].

The present paper offers a brief overview of very recent theoretical models of misfit stress relaxation in inhomogeneous crystalline nanostructures – composite nanoparticles, nanowires and nanolayers.

Mathematical tools for continuum modeling of misfit stress relaxation through generation of discrete dislocations

The invention and comparison of different relaxation micromechanisms lead to the conclusion that, in the vast majority of cases, the main channel of relaxation is the formation of various dislocation configurations [1,2,28]. To determine and analyze the critical conditions for their formation, some novel mathematical tools were developed.
In particular, new analytical solutions of the boundary problems in the theory of elasticity for circular prismatic dislocation loops in a hollow elastic sphere [29] and in an elastic cylinder [30] were obtained. Solutions were found for the strain energy of such loops [29,30] and for the energies of pair elastic interaction between them [30,31]. The stress fields and strain energy of a circular prismatic dislocation loop surrounding a cylindrical cavity in an infinite elastic medium were calculated [32] as well. All these solutions were found by using the classical methods of the elasticity theory, which were described in detail by Lurie [33]. Since the analytical formulas for the elastic fields are rather cumbersome, here we show the expressions for strain and interaction energies only that are of primary importance for theoretical modeling of the misfit-stress relaxation micromechanisms.

In the case of a circular prismatic dislocation loop placed axisymmetrically in a hollow elastic sphere (Fig. 1(a)), the elastic strain energy of the system is given by the superpositions [29]:

$$E_{\text{el}} = {}^{\infty}E - \pi b \int_0^c \tilde{\sigma}_{zz}|_{z=z_0} r dr, \; |z_0| \geq a_p, \tag{1}$$

$$E_{\text{el}} = {}^{\infty}E - \frac{Gb^2 c_p^2}{(1-\nu)c} \mathrm{D}\left(\frac{c_p}{c}\right) - \pi b \int_0^c \tilde{\sigma}_{zz}|_{z=z_0} r dr, \; |z_0| < a_p, \tag{2}$$

where ${}^{\infty}E$ is the elastic strain energy of the loop in an infinite elastic medium, b is the Burgers vector magnitude of the loop, c is the loop radius, z_0 is its position in the sphere, a_p is the radius of the cavity in the center of the sphere, G and ν are the shear modulus and the Poisson ratio, respectively, of the sphere material, $c_p = (a_p^2 - z_0^2)^{1/2}$, $\mathrm{D}(k) = \int_0^{\pi/2} \sin^2 t \, (1 - k^2 \sin^2 t)^{-1/2} dt$ is the elliptic integral [34], and $\tilde{\sigma}_{zz}$ is the axial component of the additional stress tensor that provides the fulfilment of traction-free boundary conditions on the inner and outer surfaces of the hollow sphere.

The elastic strain energy ${}^{\infty}E$ reads [35,36]:

$${}^{\infty}E = \frac{\pi G b^2 c}{2(1-\nu)} J(1,1;0)|_{r=c-r_{core}, z=z_0}, \tag{3}$$

where $J(1,1;0)|_{r=c-r_{core},z=z_0} = \int_0^{\infty} J_1(\kappa) J_1(\kappa(1 - r_{core}/c)) d\kappa$ is the Lipschitz-Hankel integral [37], $J_1(t)$ is the Bessel function of the first order, and r_{core} is the dislocation core radius. When $c >> r_{core}$, Eq. (3) is well approximated by the following equation:

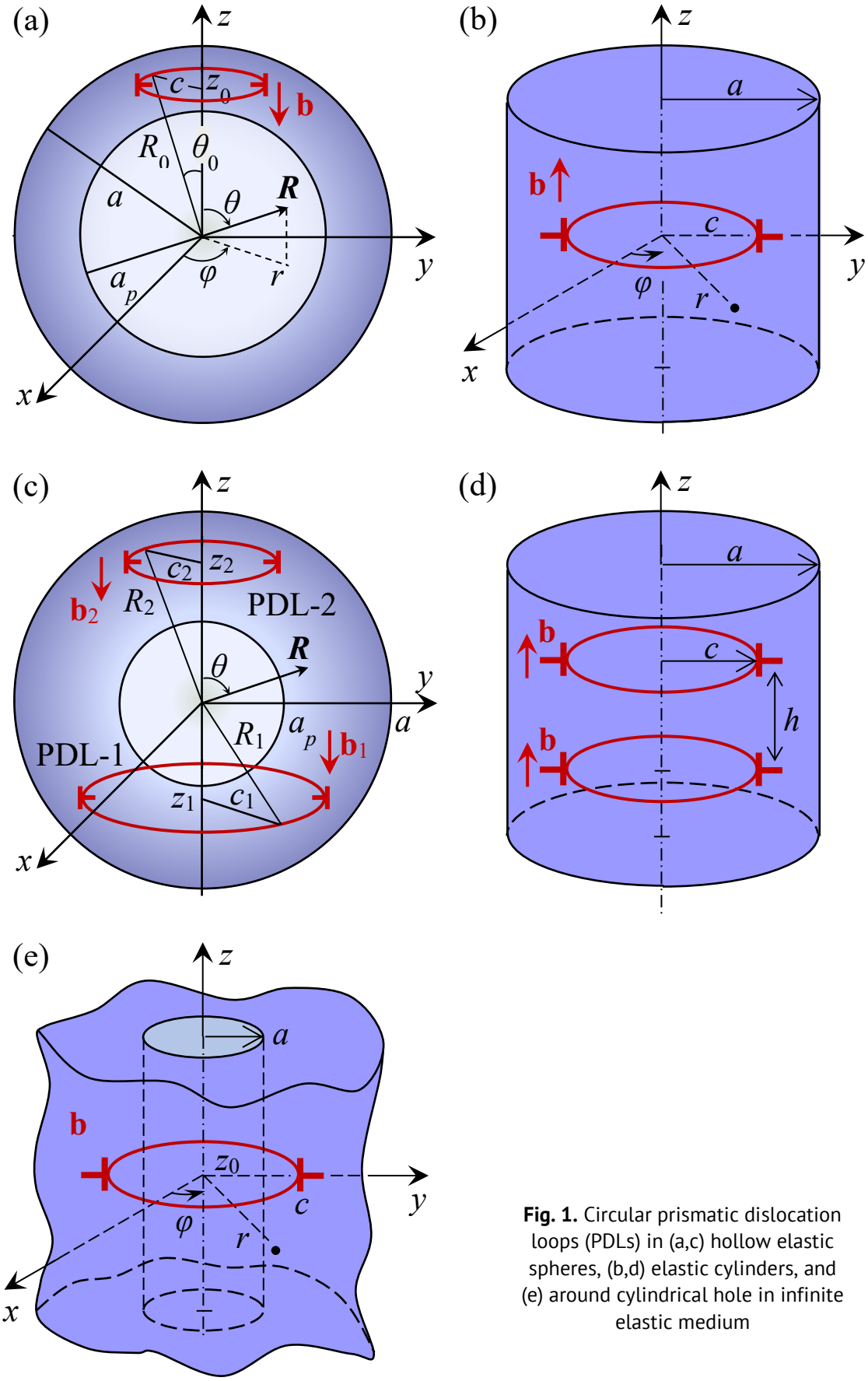

Fig. 1. Circular prismatic dislocation loops (PDLs) in (a,c) hollow elastic spheres, (b,d) elastic cylinders, and (e) around cylindrical hole in infinite elastic medium

$$^{\infty}E = \frac{Gb^2c}{2(1-\nu)}\ln\left(\frac{8c}{r_{core}} - 2\right). \quad (4)$$

The additional axial stress $\tilde{\sigma}_{zz}$ [29] is:

$$\tilde{\sigma}_{zz} = \tilde{\sigma}_{RR}\cos^2\theta + \tilde{\sigma}_{\theta\theta}\sin^2\theta - \tilde{\sigma}_{R\theta}\sin 2\theta, \quad (5)$$

with $\tilde{\sigma}_{RR} = 2G\sum_{k=0}^{\infty}\Big[A_k^{(1)}(k+1)(k^2-k-2-2\nu)R^k + B_k^{(1)}k(k-1)R^{k-2} - \frac{C_k^{(2)}k}{R^{k+1}}(k^2+3k-2\nu) + \frac{D_k^{(2)}(k+1)(k+2)}{R^{k+3}}\Big]P_k(\cos\theta)$, $\tilde{\sigma}_{R\theta} = 2G\sum_{k=0}^{\infty}\Big[A_k^{(1)}(k^2+2k-1+2\nu)R^k + B_k^{(1)}(k-1)R^{k-2} + \frac{C_k^{(2)}}{R^{k+1}}(k^2-2+2\nu) - \frac{D_k^{(2)}(k+2)}{R^{k+3}}\Big]\frac{dP_k(\cos\theta)}{d\theta}$, $\tilde{\sigma}_{\theta\theta} = 2G\sum_{k=0}^{\infty}\Big\{\Big[-A_k^{(1)}(k+1)(k^2+4k+2+2\nu)R^k - B_k^{(1)}k^2R^{k-2} + \frac{C_k^{(2)}k}{R^{k+1}}(k^2-2k-1+2\nu) - \frac{D_k^{(2)}(k+1)^2}{R^{k+3}}\Big]P_k(\cos\theta) - \Big[A_k^{(1)}(k+5-4\nu)R^k + B_k^{(1)}R^{k-2} + \frac{C_k^{(2)}}{R^{k+1}}(-k+4-4\nu) + \frac{D_k^{(2)}}{R^{k+3}}\Big]\frac{dP_k(\cos\theta)}{d\theta}\cot\theta\Big\}$.

Here R is the radial coordinate (see Fig. 1(a)), θ is the polar angle, and $P_k(t)$ are the Legendre polynomials. The coefficients $A_k^{(1)}, B_k^{(1)}, C_k^{(2)}$, and $D_k^{(2)}$ are found from the free-traction boundary conditions of the problem [29].

The graphical representation of the elastic strain energy E_{el} is given in [29]. When a circular prismatic dislocation loop is placed axisymmetrically in an elastic cylinder (Fig. 1(b)), the elastic strain energy of the system is given by the superposition [30]:

$$E_{el} = {}^{\infty}E - \frac{Gb^2at^2}{1-\nu}\int_0^{\infty}\frac{s^2t^2I_0^2(ts)+wI_1^2(ts)-2stI_1(ts)I_0(ts)[wI_1(s)K_1(s)+s^2I_0(s)K_0(s)]}{s^2I_0^2(s)-wI_1^2(s)}ds, \quad (6)$$

where $t = c/a$, $w = s^2 + 2(1-\nu)$, $I_{0,1}(\kappa)$ and $K_{0,1}(\kappa)$ are the modified Bessel functions of the first kind and the Macdonald functions, respectively.

The graphical representations of the elastic strain energy E_{el} for the circular prismatic dislocation loops in a hollow sphere and in a cylinder are given in [29,30].

The energy of pair elastic interaction between two coaxial circular prismatic dislocation loops (denoted as PDL-1 and PDL-2) in a hollow sphere (Fig. 1(c)) can be written as a sum [31]:

$$E_{int} = {}^{\infty}E_{int} + {}^{*}E_{int}, \quad (7)$$

where the first term, ${}^{\infty}E_{int}$, is the interaction energy of the loops in an infinite elastic medium, while the second term, ${}^{*}E_{int}$, is caused by the effect of the inner and outer free surfaces of the sphere.

As shown in [31], the term ${}^{\infty}E_{int}$ reads:

$$^{\infty}E_{int} = \frac{\pi Gb_1b_2}{1-\nu}\left[rJ(1,1;0) + \frac{|z-z_2|}{c_2}rJ(1,1;1)\right]\begin{matrix} r = c_1 \\ r = \xi \end{matrix}\Bigg| z = z_1, \quad (8)$$

where b_1 and b_2 are the Burgers vector magnitudes of the loops, c_1 and c_2 are their radii, z_1 and z_2 are their coordinates with respect to the sphere center (Fig. 1(c)); $\xi = 0$ for $z_1 \geqslant a_p$, and $\xi = \sqrt{a_p^2 - z_1^2}$ for $z_1 < a_p$, and $J(m,n;p) = \int_0^{\infty}J_m(\kappa)J_n(\kappa r/c_2)\exp[-\kappa|z-z_2|/c_2]\kappa^p d\kappa$.

The term ${}^{*}E_{int}$ is given by [31]:

$$^{*}E_{int} = \frac{\pi Gb_1b_2}{1-\nu}\sum_{n=0}^{+\infty}\Big[A_n^{(2)}\frac{2(n+1)(1+\nu-2n\nu-2n^2)}{2n-1}Q_{n,1} + A_{n+2}^{(2)}\frac{(n+2)(n+3)(2n^2+9n+7)}{2n+3}{}_{n,2}I_{int} + B_{n+2}^{(2)}(n+1)(n+2)Q_{n,1} - C_n^{(2)}\frac{2n[2n^2+2n(2-\nu)+1-3\nu]}{2n+3}T_{n,1} - -C_{n-2}^{(2)}\frac{n(n-2)(2n^2-7n+5)}{2n-1}T_{n,3} + D_{n-2}^{(2)}n(n-1)T_{n,3}\Big], \quad (9)$$

where $A_n^{(2)}$, $B_n^{(2)}$, $C_n^{(2)}$, and $D_n^{(2)}$ are the coefficients determined in [29] from the boundary conditions on the free inner and outer spherical surfaces, $Q_{n,l}$ and $T_{n,l}$ are the following polynomials:

$$Q_{n,l} = \sum_{s=0}^{[n/2]} \frac{(-1)^s}{2^{n(s+l)}} \binom{n}{s} \binom{2n-2s}{n} z_1^{n-2s} (R_1^{2(s+l)} - \zeta^{2(s+l)}), \tag{10a}$$

$$T_{n,l} = \sum_{s=0}^{[n/2]} \frac{(-1)^s}{2^{n(-2k+2s+l)}} \binom{n}{s} \binom{2n-2s}{n} z_1^{n-2s} (R_1^{-2k+2s+l} - \zeta^{-2k+2s+l}). \tag{10b}$$

Here $[n/2]$ denotes the greatest integer $\leq n/2$, $\binom{n}{s}$ are the binomial coefficients, and $\zeta = z_1$ for $z_1 \geqslant a_p$, and $\zeta = a_p$ for $z_1 < a_p$.

In a cylinder of radius a (Fig. 1(d)), the energy of pair elastic interaction between two identical axisymmetric circular prismatic dislocation loops of radius c with the Burgers vector magnitude b and spacing h is given by the sum (7), the terms of which can be written as follows [30]:

$${}^{\infty}E_{\text{int}} = \frac{\pi G b^2 c}{1-\nu} \left(J(1,1;0) \rightleftarrows|_{z=h} + \frac{h}{c} J(1,1;1)|_{z=h} \right), \tag{11a}$$

$${}^{*}E_{\text{int}} = \frac{2Gb^2ct}{1-\nu} \int_0^{\infty} \frac{s^2t^2I_0^2(ts) + wI_1^2(ts) - 2stI_1(ts)I_0(ts)[wI_1(s)K_1(s) + s^2I_0(s)K_0(s)]}{s^2I_0^2(s) - wI_1^2(s)} \cos\frac{hs}{a} ds\,. \tag{11b}$$

The interaction energies for the circular prismatic dislocation loops in a hollow sphere and in a cylinder are illustrated in detail by maps [31] and plots [30], respectively.

The total (including the energy of the dislocation core) energy of a circular prismatic dislocation loop surrounding a cylindrical cavity in an infinite elastic medium (Fig. 1(e)) [32] is:

$$E_t = \frac{Gb^2c}{2(1-\nu)} \left\{ \ln\frac{1.08\gamma c}{b} - \frac{2}{t}\mathbf{D}\left(\frac{1}{t}\right) - 2\int_0^{\infty} \{(-2A_1\nu + B_1\beta)[K_1(\beta) - tK_1(\beta t)] + \right.$$
$$\left. + A_1\beta[K_2(\beta) - t^2K_2(\beta t)]\} d\beta \right\}, \tag{12}$$

where the first term is the total energy of the loop in an infinite elastic medium [36,38], γ is the core energy parameter ranging from 1 for metals to 4 for semiconductors [38] and the coefficients A_1 and B_1 are given by the following equations [32]:

$$A_1 = \pm \frac{K_1(\beta t)[wI_1(\beta)K_1(\beta) + \beta^2 I_0(\beta)K_0(\beta)] - \beta t K_0(\beta t)}{wK_1^2(\beta) - \beta^2 K_0^2(\beta)}, \tag{13a}$$

$$B_1 = \pm \left\{ \frac{tK_0(\beta t)[wI_1(\beta)K_1(\beta) + \beta^2 I_0(\beta)K_0(\beta) + 2 - 2\nu]}{wK_1^2(\beta) - \beta^2 K_0^2(\beta)} + \right.$$
$$\left. + \frac{K_1(\beta t)\{2(\nu-1)[\beta^2 I_0(\beta)K_0(\beta) + wI_1(\beta)K_1(\beta)] - w\}}{\beta[wK_1^2(\beta) - \beta^2 K_0^2(\beta)]} \right\}. \tag{13b}$$

Here $w = \beta^2 + 2(1-\nu)$.

The energy plots illustrating Eq. (12) are represented in Ref. [32] in detail.

Critical conditions for the onset of misfit dislocations in core-shell nanoparticles

Using the solutions for the self strain energies of circular prismatic dislocation loops placed in elastic bodies of different geometry (see the previous section), the critical conditions necessary for the formation of circular prismatic misfit dislocation loops (MDLs) at the interfaces in core-shell nanoparticles with different types of cores were determined. In particular, the critical conditions for the formation of MDLs in solid [39,40] and hollow [41] single-crystalline and in solid decahedral [42] spherical nanoparticles were considered. To model the latter, a new solution for the elastic fields of a wedge disclination in an elastic sphere [43] was used. The cases of cores in the form of a

solid [39,42] and hollow [41] sphere, as well as in the form of a hemisphere resting on the equatorial plane of a nanoparticle [40] were investigated.

Within the continuum approach, the calculation scheme was based on the assumption that the difference in the total energy of the system under study ΔE due to the onset of the first MDL can be approximated by the following general formula [44]:

$$\Delta E = E_{\text{el}} + E_{\text{c}} + E_{\text{int}}, \tag{14}$$

where E_{el} is the elastic strain energy of the MDL in the system, E_{c} is the energy of the MDL core, and E_{int} is the energy of interaction of the MDL with the initial misfit stress in the system before the MDL appearance there.

The formation of the first MDL is energetically favorable if $\Delta E < 0$. Therefore, the equation $\Delta E = 0$ gives the critical conditions for its onset in the system. Since the energy difference ΔE (more precisely, its third term E_{int}) is always in linear proportion with the misfit parameter f (here we assume for definiteness that $f > 0$), this equation is always simply resolved with respect to a critical misfit f_c given by:

$$f_c = -\frac{E_{\text{el}}+E_{\text{c}}}{E^*_{\text{int}}}, \tag{15}$$

where $E^*_{int} = E_{int}/f$. Thus, the critical (necessary) condition for the formation of the first MDL in the system can be written as $f > f_c$. As a result, the analyzes of the system stability with respect to its transition from the coherent state (with no MDL) to the partly relaxed (semicoherent) state with a MDL comes down to studying the dependences of the critical misfit f_c on other parameters (geometric, material, etc.) of the system.

Consider, for example, the case of a spherically symmetric core-shell nanoparticle studied in [39]. It was assumed that the nanoparticle consisted of an elastically isotropic core and an elastically isotropic shell with identical elastic moduli but different lattice parameters a_1 and a_2 (Fig. 2(a)). The lattice misfit was defined by the parameter $f = 2(a_1 - a_2)/(a_1 + a_2) > 0$. The outer and inner radii of the shell were denoted by a and R_0, respectively. During the coherent growth of the shell on the core, misfit strains and stresses should appear in the core-shell nanoparticle [1,2]. For some values of the system parameters f, a, and R_0, the interface was supposed to transform into a semicoherent state corresponding to the formation of a misfit dislocation at it. Owing to the spherical

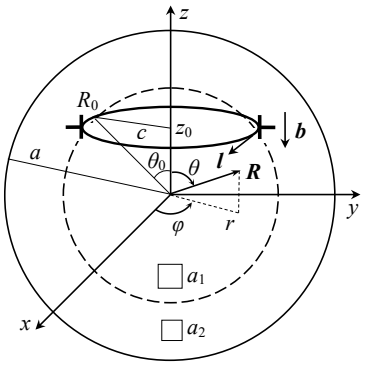

Fig. 2. Model of a circular MDL with the Burgers vector **b** and the tangent vector ***l*** at the interface in a core-shell nanoparticle. The spherical (R, φ, θ), cylindrical (r, φ, z) and Cartesian (x, y, z) coordinate systems are shown. The geometric parameters of the system are the nanoparticle radius a, the nanoparticle core radius R_0, the MDL radius c, and the MDL coordinate z_0. The lattice parameters a_1 and a_2 satisfy the inequality $a_1 > a_2$. Adopted from [39]

symmetry of the system, it was expected the formation of a vacancy (for $f > 0$) MDL around the core, which would partially compensate the lattice misfit. It is worth noting that earlier this problem got an approximate solution [2,12] for the case when the MDL was located in the equatorial plane of the nanoparticle and the core and shell were characterized by different elastic moduli.

In the elastically homogeneous case [39], the first term $E_{\rm el}$of the energy difference ΔE given by Eq. (14) can be derived from Eq. (1) in the limiting case of $a_p \to 0$. The second and third terms of ΔE are [39]:

$$E_{\rm c} \approx \frac{Gcb^2 Z}{2(1-\nu)}, \tag{16}$$

$$E_{\rm int} = -\frac{4\pi}{3}\frac{1+\nu}{1-\nu} Gbc^2 f\left(1 - \frac{{R_0}^3}{a^3}\right), \tag{17}$$

where $Z = \ln\alpha$ and the parameter α can vary in the range from 1 to 4 when $r_{core} = b$ [38]. In numerical calculations of [39], it was assumed that $Z = 1$.

Introduction of Eq. (1) at $a_p \to 0$ with Eqs. (4), (5), (16) and (17) to Eq. (15) gave an analytical formula for the critical misfit f_c [39]. Figure 3 shows the dependences of f_c on the principal geometric parameters of the system: (a) the normalized position z_0/R_0 of the MDL for the two different outer radii of the nanoparticles $a = 50b$ (solid curves) and $200b$ (dashed curves) with different values of the normalized core radius R_0/a and (b) the normalized core radius R_0/a for different values of the nanoparticle radius a at $z_0 = 0$ (here the solid and dashed curves correspond to the strict [39] and approximate [2,12] solutions, respectively). Each of these curves separates the phase space (R_0/a, f_c) into two regions. In the region under the curve, the MDL formation is energetically unfavorable, while in the region above the curve, it is energetically favorable. As is seen from Fig. 3(a), for any value of R_0/a, the minimum value of f_c is reached for the MDL position in the equatorial plane of the nanoparticle ($z_0 = 0$). Therefore, the first MDLs are expected to form in equatorial sections of the nanoparticles.

In Fig. 3(b), the dashed curves correspond to the approximate solutions obtained in [2,12] for a thin shell on a massive core ($R_0/a \to 1$) and for a massive shell on a small core ($R_0/a \ll 1$). It is seen that the strict solution (15) coincides almost completely with the approximate solution for large nanoparticles and differs significantly from it for small nanoparticles, when the approximate solution somewhat overestimates the critical misfit parameter f_c.

For a fixed misfit parameter f, which, in the diagram (R_0/a, f_c), is represented by the horizontal line, the points of intersection $f = f_c$ determine the critical values of the normalized core radius $\tilde{R}_0 = R_0/a$. The critical normalized radii $\tilde{R}_{0,\,c1}$ and $\tilde{R}_{0,\,c2}$ are such that the generation of an MDL is possible only in the range $\tilde{R}_{0,\,c1} < \tilde{R}_0 < \tilde{R}_{0,\,c2}$ and impossible neither for the extremely small core ($\tilde{R}_0 < \tilde{R}_{0,\,c1}$) nor for the extremely thin shell ($\tilde{R}_0 > \tilde{R}_{0,\,c2}$). For example, at $f_c = 0.01$ and $a = 200b$, the critical values of the normalized radii of the cores are $\tilde{R}_{0,c1} \approx 0.225$ and $\tilde{R}_{0,c2} \approx 0.935$ (Fig. 3(b)). In absolute units, these estimates give $R_{0,c1} \approx 45b$ and $R_{0,c2} \approx 187b$.

It is also seen from Fig. 3(b) that, for a given particle size, there is a minimum critical misfit $f_{c,\min}$, such that at $f < f_{c,\min}$, in the particle with a radius a the MDL generation is energetically unfavorable for any value of the ratio R_0/a. For example, $f_{c,\min} \approx 0.005$ for the curve with $a = 200b$ and $f_{c,\min} \approx 0.014$ for the curve with $a = 50b$.

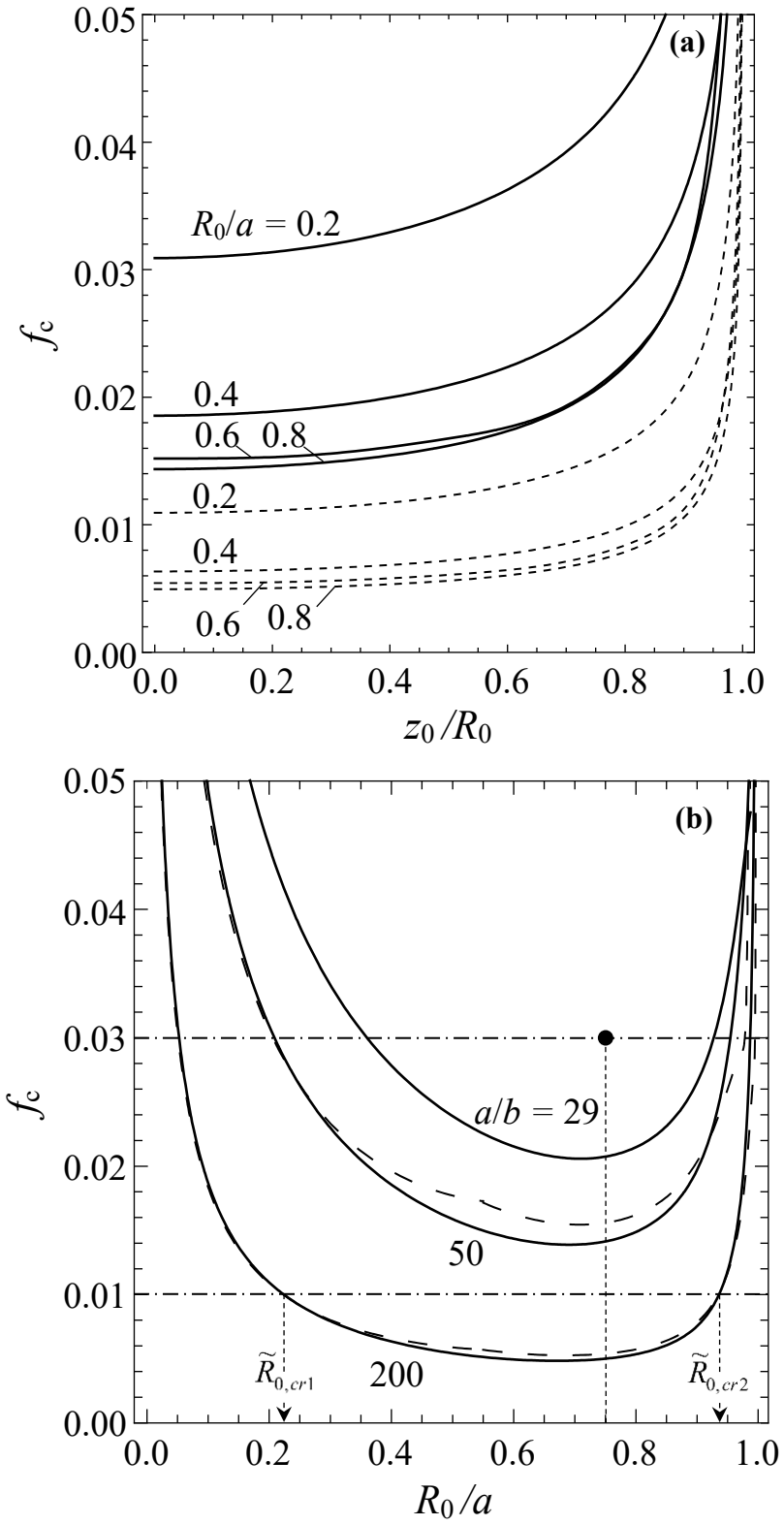

Fig. 3. Dependences of the critical misfit f_c on the geometric parameters of the system: (a) the normalized MDL position z_0/R_0 for the nanoparticle radii $a = 50b$ (solid curves) and $200b$ (dashed curves) with different values of the normalized core radius R_0/a and (b) the normalized core radius R_0/a for different values of the nanoparticle radius a at $z_0 = 0$ (the solid and dashed curves correspond to the strict [39] and approximate [2,12] solutions, respectively). The point (0.75, 0.03) corresponds to the experimental observation of a perfect MD in the Au-$FePt_3$ nanoparticle with radius $a = 29b$ [45]. Adopted from [39]

The point with coordinates (0.75, 0.03) in Fig. 3(b) corresponds to the experimental observation of a perfect edge MD in the Au-$FePt_3$ nanoparticle with radius a = 29b [45]. It is seen that this point lies in the region $f > f_c(R_0/a)$ where the generation of MDLs was predicted by the calculations [39].

A similar problem for a hollow core-shell nanoparticle was solved in work [41]. Figure 4 shows the corresponding model of a circular MDL placed at the core-shell interface in the plane $z = z_0$. In this case, the difference in the total energy of the system ΔE due to the onset of the first MDL was approximated by Eq. (14), in which the first term was given by Eqs. (1) and (2), the second term by Eq. (16) and the third term by [41]:

$$E_{int} = -\frac{4\pi}{3}\frac{1+\nu^2}{1-\nu}\left(1-\frac{R_0^3}{a^3}\right)\frac{1-(a_p/R_0)^3}{1-(a_p/a)^3}. \quad (18)$$

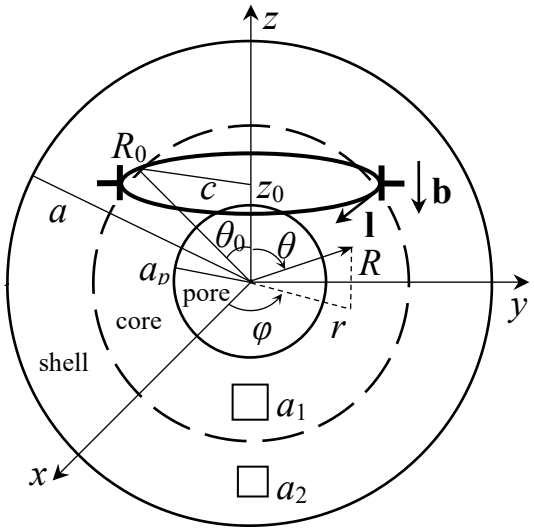

Fig. 4. Model of a circular MDL with the Burgers vector **b** and the tangent vector $\boldsymbol{l}$ at the interface in a hollow core-shell nanoparticle. The spherical (R, φ, θ), cylindrical (r, φ, z) and Cartesian (x, y, z) coordinate systems are shown. The geometric parameters of the system are the nanoparticle radius a, the nanoparticle core radius R_0, the pore radius a_p, the MDL radius c, and the MDL coordinate z_0. The lattice parameters a_1 and a_2 satisfy the inequality $a_1 > a_2$. Adopted from [41]

In the limit $a_p \to 0$, Eq. (18) transforms to Eq. (17). As a result, the critical condition for the MDL formation is given in this case by the inequality $f > f_c$, where the critical misfit f_c is determined by Eq. (15).

Figure 5(a) shows the dependence $f_c(z_0/R_0)$ for $a = 100b$, $R_0/a = 0.8$, and different values of the ratio a_p/a. It is seen that f_c increases both with z_0/R_0 and a_p/a ratios. It means that the most favorable position of the MDL is in the equatorial plane of a hollow core-shell nanoparticle as is also the case with solid core-shell nanoparticles [39]. It is also seen than both the MDL shift from the equatorial plane and pore growth in the core decrease the energetic preference of the MDL generation in hollow core-shell nanoparticles.

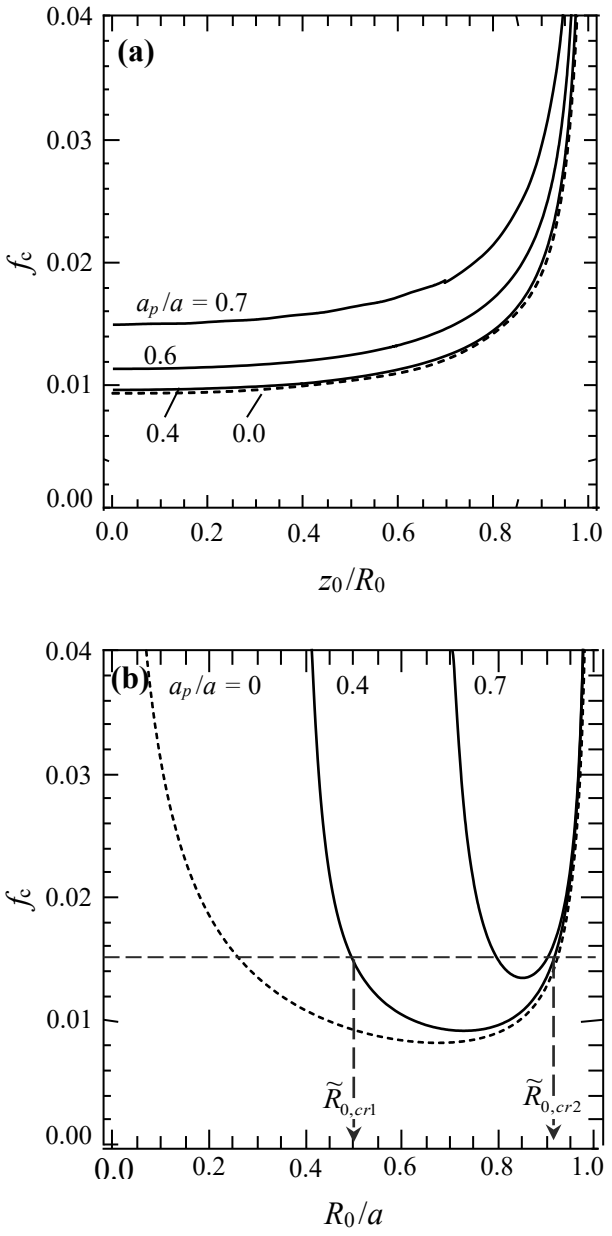

Fig. 5. Dependence of the critical misfit f_c of a hollow core-shell nanoparticle with outer radius $a = 100b$ on (a) the normalized MDL position z_0/R_0 for the fixed normalized core radius $R_0/a = 0.8$, and (b) the normalized core radius R_0/a for the equatorial position ($z_0 = 0$) of the MDL, for different values of the normalized pore radius a_p/a. The dashed curves correspond to full core-shell nanoparticles. Adopted from [41]

Figure 5(b) illustrates the effect of the $R_0/a = \tilde{R}_0$ ratio on the critical misfit f_c. Here the curves $f_c(\tilde{R}_0)$ were plotted for $a = 100b$, $z_0 = 0$, and different values of a_p/a. They have minima which give the minimal critical misfit $f_{c,\min}$ such that no MDL can form at $f < f_{c,\min}$for any $\tilde{R}_0$. For $f > f_{c,\min}$, there is a range $\tilde{R}_{0,\,c1} < \tilde{R}_0 < \tilde{R}_{0,\,c2}$, in which MDL generation is energetically favorable. When $\tilde{R}_0 < \tilde{R}_{0,\,c1}$ or $\tilde{R}_0 > \tilde{R}_{0,\,c2}$, the coherent state of the nanoparticle is more preferable. With raising *f*, this range increases. Similar results were reported earlier for MDLs in solid core-shell nanoparticles [39] (see also the above

discussion of Fig. 3(b)) and straight MDs in solid core-shell nanowires [46] and at the interface between a (nano)tube and surrounding infinite matrix [47]. As is seen, the pore strongly affects the curves $f_c(\tilde{R}_0)$: they become narrower with increasing the pore radius a_p, and $f_{c,min}$ increases as well. As a result, the range $(\tilde{R}_{0,c1}, \tilde{R}_{0,c2})$ decreases. Thus, the region of parameter values, in which the MDL formation is energetically favorable, drastically shrinks.

The most important practical issues from the model [41] are the dependences of the minimal critical misfit $f_{c,min}$ and the critical shell thickness $h_c = a(1 - \tilde{R}_{0,c2})$ on the ratio a_p/a (Fig. 6). It is seen from Fig. 6 that both $f_{c,min}$ and h_c weakly depend on the a_p/a ratio until it reaches the value of about 0.8. However, when $a_p/a > 0.8$, they drastically grow with a_p/a. The authors of [41] concluded on a great potential in developing coherent (MD free) hollow core-shell nanoparticles by using cores in the form of thin-wall shells with the inner-to-outer radii ratio larger than 0.8.

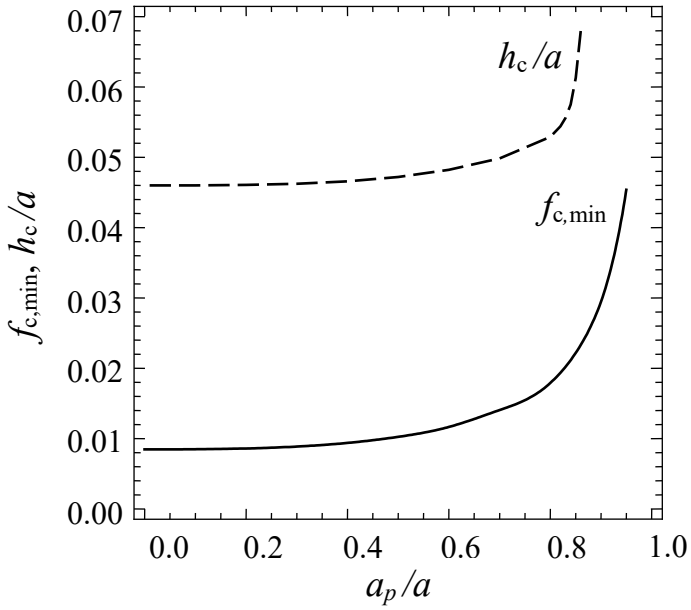

Fig. 6. Dependences of the minimal critical misfit $f_{c,min}$ and the critical shell thickness h_c (at $f = 0.02$) on the inner-to-outer radii ratio a_p/a for $a = 100b$ and $z_0 = 0$. Adopted from [41]

The solid and hollow core-shell nanoparticles considered in [39,41] were supposed single crystalline (solid and hollow SC-CSNPs). Krauchanka et al. [42] extended this energetic approach to the case of solid decahedral core-shell nanoparticles (Dh-CSNPs). Indeed, the most of bimetallic CSNPs contain noble metals (Au, Ag, Pt and Pd) whose nanoparticles are well known to be so-called pentagonal nanoparticles (PNPs) in the greater part of their populations.

PNPs are multiply-twinned crystalline particles in the shape of either decahedron or icosahedron, or of close morphologies [48–51]. As a result, PNPs possess five-fold symmetry axes that are absent in bulk single crystals and pass through quintuple junctions of twin boundaries. These axes can be described in terms of positive partial wedge disclinations (WDs). For example, decahedral particles (DhPs) contain one WD [52], while icosahedral particles (IcPs) contain six WDs [53]. Due to these WDs, PNPs are

elastically strained and store high strain energy that can relax through generation of various lattice defects [48,50,51].

The elastic model of a spherical DhP can be given by a partial positive WD piercing the elastic sphere [43]. In solid DhPs, the WD stress relaxation was shown to occur through the generation of axisymmetric circular PDLs [54]. For hollow DhPs, a model was suggested that described the formation of multiple cracks at the twin boundaries with subsequent agglomeration of the initial cracks into a unite five-foldstar crack [55].

For a Dh-CSNP that is a DhP covered with a shell of another crystalline material, the superpositions of the WD and misfit strains and stresses were expected [42]. The stress/strain state of a WD axially pierced an elastic sphere (Fig. 7(a)) was given in [43]. The authors [43] showed that in the area around the line of a positive WD is hydrostatically compressed, while the peripheral area of the sphere is hydrostatically stretched. They suggested that stress relaxation in the system could naturally include nucleation of vacancies at the stretched surface of the sphere, their migration to the compressed region around the WD line, and their coagulation with formation of a circular PDL of vacancy type [54].

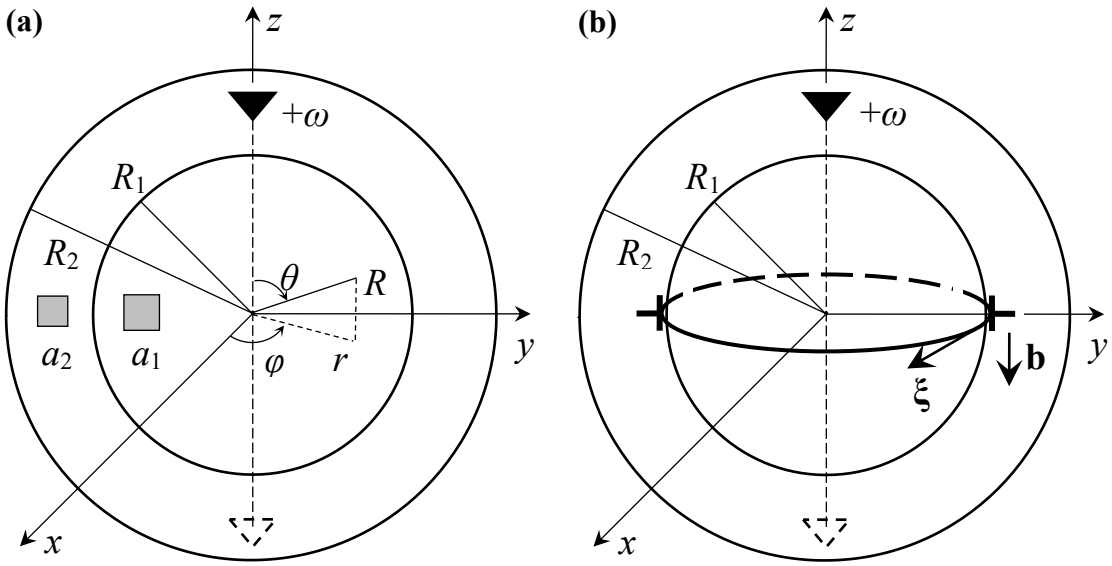

Fig. 7. Model of a Dh-CSNP in its (a) initial and (b) partially relaxed states. The Cartesian (x, y, z), cylindrical (r, φ, z) and spherical (R, ϑ, φ) coordinate systems are shown. Adopted from [43]

In a Dh-CSNP with $f > 0$ (Fig. 7(a)), the formation of such a PDL could be effective for both the WD and misfit stress/strain states (Fig. 7(b)). Since the equatorial planes are the most favorable positions for MDLs and PDLs in SC-CSNPs [39,41] and DhPs [54], respectively, it was suggested that the equatorial plane is the most favorable position of a MDL in a Dh-CSNP, too [43]. In this case, the total energy change caused by the partial relaxation in a Dh-CSNP reads [43]:

$$\Delta E = E_{\mathrm{c}} + E_{\mathrm{el}} + E_{\mathrm{int},\nabla} + E_{\mathrm{int,f}} + E_{\mathrm{st}}, \tag{19}$$

where the first two terms are the core and strain energies of the MDL, respectively, as before; $E_{\mathrm{int}\nabla}$ and $E_{\mathrm{int,f}}$ are the energies of interaction of the MDL with the WD and

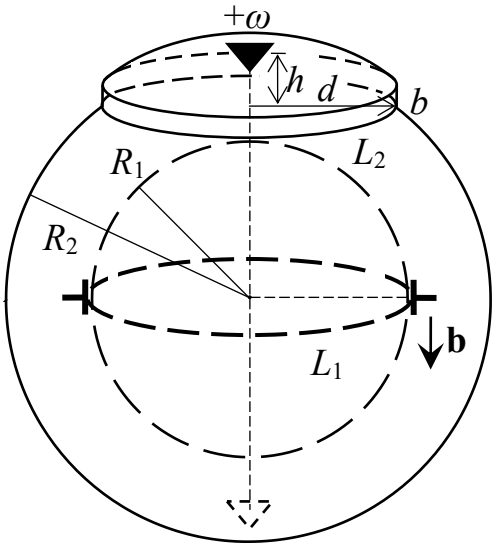

Fig. 8. Formation of a circular MDL of length L_1 with the Burgers vector **b** in the Dh-CSNP leads to the formation of a monolayer with a step of radius d, height b and length L_2 around a pole on the free surface of the shell. Adopted from [43]

misfit stresses, respectively; and E_{st} is the energy of the atomic step that forms on the Dh-CSNP free surface in the process of the generation of vacancies needed for the MDL creation (Fig. 8).

The interaction energy $E_{\text{int},\nabla}$ is [54]:

$$W_{\text{int},\nabla} = 2\pi DbR_1^2\omega \left[\nu \ln\frac{t}{2} + \frac{21+\nu(238+125\nu)}{30(7+5\nu)} - \frac{(7+\nu)(1+3\nu)}{8(7+5\nu)}t^2 - \right.$$
$$\left. - \sum_{m=2}^{+\infty}\left(\tilde{A}_m\frac{(2m+1)(2m^2+4m+1+\nu)}{m+1} + \tilde{B}_m\frac{2m}{t^2}\right) t^{2m}P_{2m}(0)\right]. \quad (20)$$

where R_1 and R_2 are the core and shell radii, respectively, of the Dh-CSNP (Fig. 7), $t = R_1/R_2$, ω is the strength of the WD, $\tilde{A}_m = \frac{\sigma_m - 2m\tau_m}{2s_m}$, $\tilde{B}_m = -\frac{p_m\sigma_m + 2q_m\tau_m}{2(2m-1)s_m}$, $\sigma_m = (2m - -1)(m+1)\tau_m - \frac{4m+1}{2m(2m+1)}$, $\tau_m = \frac{(1-2\nu)(4m+1)}{2(m-1)m(2m+1)(2m+3)}$, $s_m = 1+\nu+2m(1+2m+2\nu)$, $p_m = = 2\nu - 1 + 4m(1+m)$, $q_m = 1+\nu-4m^3+(3+2\nu)m$, and $m = 2,3,4, \ldots$.

The interaction energy $E_{\text{int,f}}$ is given by [54] $E_{\text{int,f}} = -(8/3)\pi^2 Df(1+\nu)bR_1^2(1-t^3)$. The surface step energy E_{st} was estimated as [54] $E_{\text{st}} \approx \kappa\pi Db^2R_1\sqrt{1-t^2/4}$ with $\kappa \leq 1$. It is worth noting that the terms like E_{st} have never been accounted for in previous theoretical models of MD formation. The authors [54] showed that it may give a strong effect on the critical conditions for this process.

When the critical conditions are formulated as in the aforementioned models [39,41] in terms of the misfit parameter value as $f > f_c$, where f_c is the minimal value of the lattice misfit for which the generation of a MDL becomes energetically favorable, the equation $\Delta E = 0$ gives [54]:

$$f_c = \frac{3(E_c + E_{\text{el}} + E_{\text{int},\nabla} + E_{\text{st}})}{8\pi^2(1+\nu)DbR_1^2(1-t^3)}. \quad (21)$$

Figure 9 shows the dependence of f_c on the ratio t for the following set of material parameters: $\alpha = e$ (an average value in the range from 1 to 5 [38]), $\kappa = 1$, $\omega = 7°20' \approx$ ≈ 0.128 rad, and $\nu = 0.3$, for three different values of the normalized shell radius

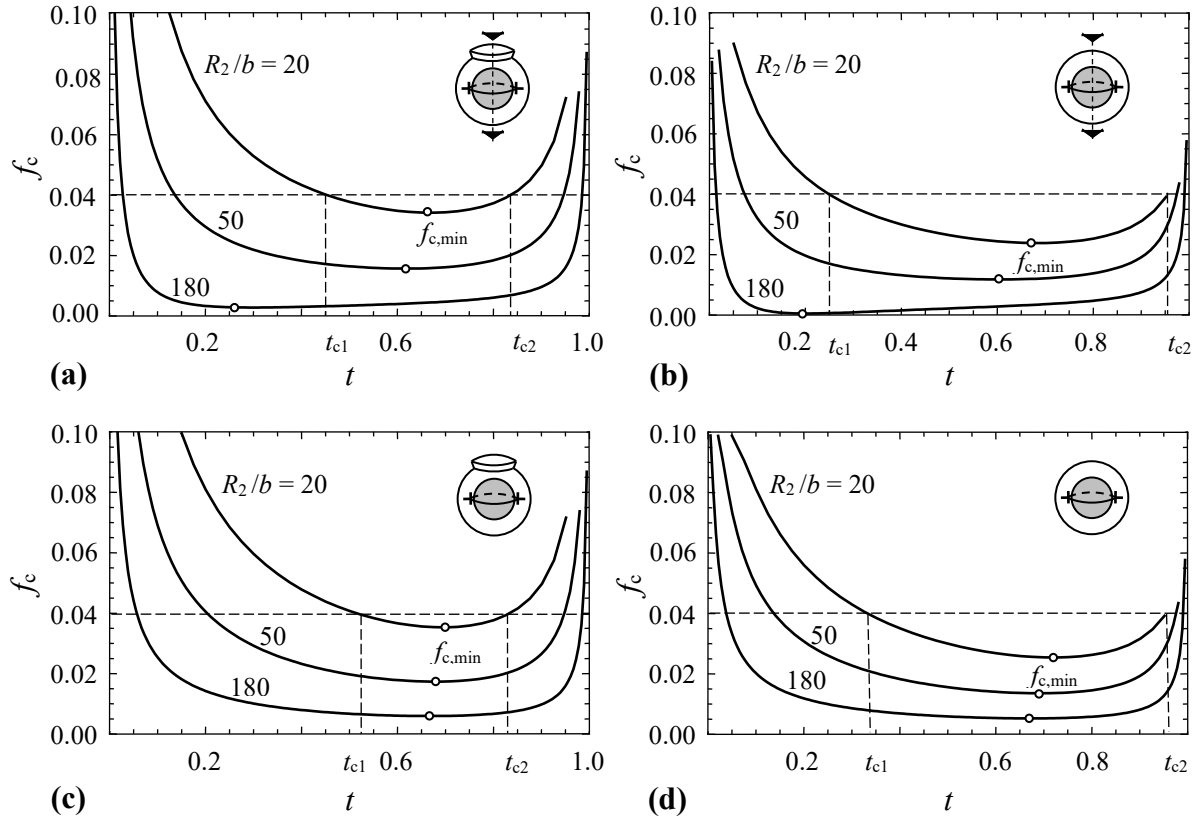

Fig. 9. The dependence of critical misfit parameter f_c on the ratio $t = R_1/R_2$ at $\alpha = e$ for nanoparticles of different size (R_2/b = 20, 50, and 180) and type, (a,b) Dh-CSNPs and (c,d) SC-CSNPs, with (a,c) and with no (b,d) account for the surface step energy. Adopted from [43]

$\frac{R_2}{b} = 20, 50$, and 180 in two cases: Fig. 9(a,b) for a Dh-CSNP (with $\omega = 0.128$ rad) and, for comparison, Fig. 9(c,d) for a SC-CSNP (with $\omega = 0$). Figures 9(a) and 9(c) illustrate the results obtained with taking into account the surface step energy term E_{st}, while Figs. 9(b) and 9(d) show those obtained without this term. One can see that the curves $f_c(t)$ are qualitatively similar for all the cases under consideration. They are also similar to the dependences calculated earlier in [39,41] (see Figs. 3(b) and 5(b)).

However, the values of the critical parameters $f_{c,min}$, t_{c1} and t_{c2} are quite different for these cases. For example, for Dh-CSNPs of radius $\frac{R_2}{b} = 20, 50$, and 180 (Fig. 9(a)), the minimum critical misfit $f_{c,min}$ ~ 0.034, 0.016, and 0.003, respectively, while in the case of SC-CSNPs of the same radii (Fig. 9(c)), $f_{c,min}$ ~ 0.036, 0.018, and 0.006, respectively. Thus, the relative difference in the $f_{c,min}$ values increase as ~ 5.9, 12.5, and 100 % with increasing value of R_2/b.

It is also seen that the interval $[t_{c1}, t_{c2}]$ where the MDL formation is energetically favorable for a given $f > f_{c,min}$ is also larger for Dh-CSNPs than for SC-CSNPs. For example, at $R_2/b = 20$ and $f = 0.04$, it is approximately $[0.45, 0.83]$ for Dh-CSNPs (Fig. 9(a)) and $[0.52, 0.83]$ for SC-CSNPs (Fig. 9(c)). As noted in [43], the interval widening in Dh-CSNPs results from the diminishing t_{c1}, while the value of t_{c2} remains practically the same for any fixed value of R_2/b. This means that t_{c1} is strongly affected by the

interaction of MDLs with WDs, modeling the five-fold symmetry axes in Dh-CSNPs, while t_{c2} is mainly controlled by the misfit relaxation in the Dh-CSNPs and SC-CSNPs.

The authors [43] also noted the different positions of the points of minimum of curves $f_c(t)$ for Dh-CSNPs and SC-CSNPs. For Dh-CSNPs, this position significantly shifts to the region of smaller t with an increase in R_2, from ~ 0.67 for $R_2 = 20b$ to ~ 0.26 for $R_2 = 180b$ (Fig. 9(a)). In contrast, this position remains almost the same, in the range of $t \approx 0.67 - 0.70$, for SC-CSNPs.

It was finally concluded [43] from Fig. 9 that Dh-CSNPs should be noticeably less stable with respect to the formation of MDLs than SC-CSNPs in the case of $f > 0$. The account for the surface step energy leads to significant correction of the $f_c(t)$ plots when the shell radius R_2 is relatively small, when the surface energy contribution E_{st} becomes comparable with other energy terms in Eqs. (19) and (21).

A comparison of the theoretical results [43] with experimental observations of perfect MDs in Dh-CSNPs and SC-CSNPs is shown in Fig. 10. In particular, Ding et al. [45] observed MDs in Au-$FePt_3$ Dh-CSNP and SC-CSNP with $f \approx 0.03$, $t \approx 0.67$ and 0.75, and $R_2 \approx 16b$ and $15b$, respectively. The corresponding blue and black points lie a little higher the blue and black curves $f_c(t)$ plotted at $\alpha = 1$ for these values of R_2, and well fall into the intervals $[t_{c1}, t_{c2}]$ for these curves at $f = 0.03$. Khanal et al. [56] observed three similar MDs in an Au-CuS_2 Dh-CSNP with $f \approx 0.11$, $t \approx 0.8$ and $R_2 \approx 74b$. The corresponding red point lies much higher the red curve $f_c(t)$ plotted at $\alpha = 1$ for this value of R_2, and obviously well falls into the interval $[t_{c1}, t_{c2}]$ for this curve at $f = 0.11$. Thus, the results of the theoretical model [43] were in a good accordance with available experimental observations of perfect MDs in Dh-CSNPs and SC-CSNPs.

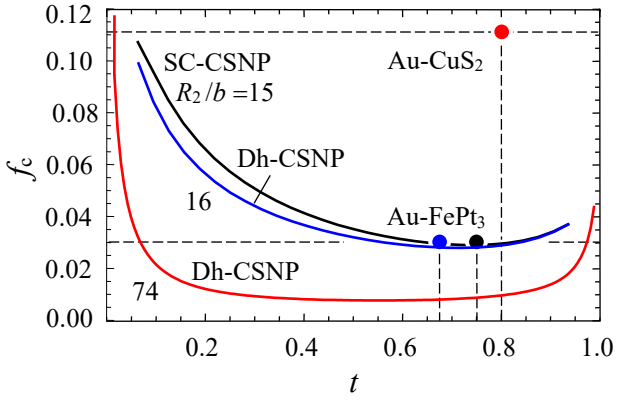

Fig. 10. Theoretical curves $f_c(t)$ for Dh-CSNPs with shell radii $R_2 = 16\,b$ (blue) and $74\,b$ (red), and SC-CSNPs with shell radius $R_2 = 15\,b$ (black), plotted for $\alpha = 1$. Experimental points (0.67, 0.03) and (0.75, 0.03) correspond to observation of perfect MDs in Au-$FePt_3$ Dh-CSNPs and SC-CSNPs, respectively [45]. Experimental point (0.8, 0.11) corresponds to observation of perfect MDs in an Au-CuS_2 Dh-CSNP [56]. Adopted from [43]

The case of a solid core in the form of a hemisphere resting on the equatorial plane of a SC-CSNP (Fig. 11) was investigated in [40]. As before, for definiteness, it was assumed that $a_1 > a_2$ and, therefore, $f > 0$. The misfit stress relaxation was supposed to occur through the transition of the SC-CSNP from the initial coherent state with no misfit defects (Fig. 11(a)) to a partly relaxed semi-coherent state, in which case a circular

prismatic MDL forms at the core-shell interface (Fig. 11(b)). The initial coherent strain/stress state in such a SC-CSNP was calculated by Kolesnikova at al. [57]. Based on this solution, the authors [40] assumed that, for $f > 0$, the MDL should be of vacancy type and could form from vacancies which nucleate on the free surface of the SC-CSNP, in the polar region of higher positive values of the elastic dilatation, and migrate to the dilatationally compressed core (see Fig. 4 in [57]).

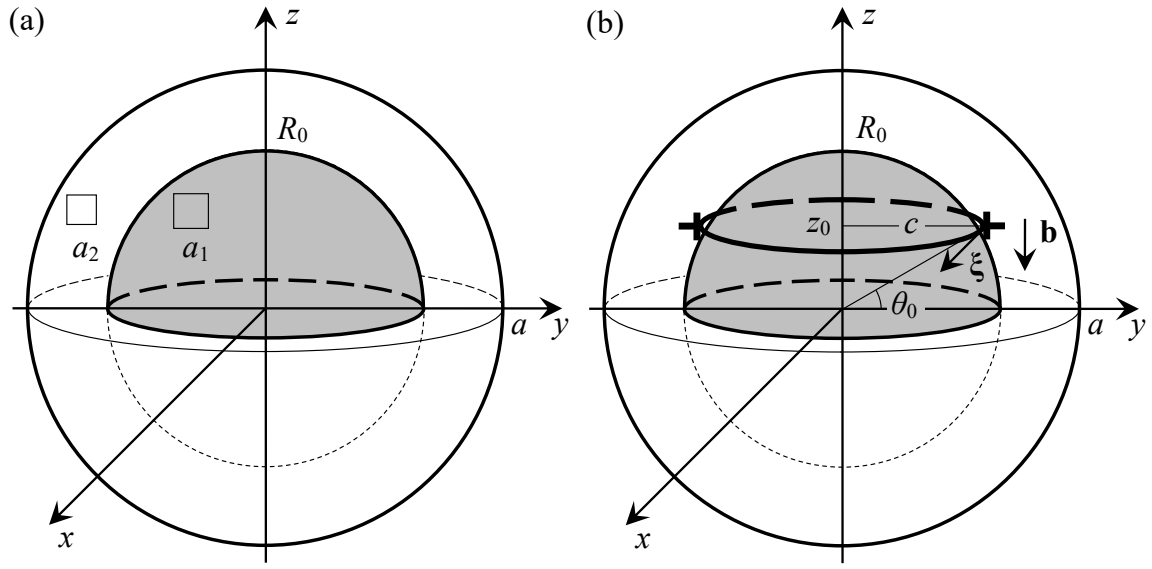

Fig. 11. Model of a SC-CSNP with an axisymmetrical semispherical core in its (a) initially coherent and (b) partially relaxed states. Adopted from [40]

The necessary condition for the MDL formation was given in [40] by the inequality $\Delta E < 0$, where the energy change ΔE is determined by Eq. (14). The first two terms on the right hand side of this equation are the strain and core energies, respectively, of the MDL as before, while the third term is the energy E_{int} of elastic interaction of the MDL with the misfit stress field in the SC-CSNP with a semispherical core. The latter was found as the work spent to generate the MDL in the axial misfit stress σ_{zz} through the integral [40]:

$$E_{\text{int}} = -\backslash\pi bz\,{}^{2}_{0}\int_0^{\theta_0}\sigma_{zz}(z=z_0)\frac{\sin\theta}{\cos^3\theta}d\theta\,, \qquad (22)$$

where b is the Burgers vector magnitude of the MDL, z_0 is the MDL position with respect to the equatorial plane of the SC-CSNP (Fig. 11(b)), and θ_0 is the angular coordinate of the MDL line.

The authors [40] calculated numerically the energy change ΔE for a model SC-CSNP with radius $a = 200b$ and Poisson ratio $\nu = 0.3$. Figure 12 shows the dependence of ΔE on the normalized coordinate z_0/R_0 of the MDL plane (here R_0 is the core radius) for different values of the misfit f and the ratio R_0/a .

In the case, when $f = 0.02$ and R_0/a is varied from 0.1 to 0.99 (Fig. 12(a)), the curves allow to predict the energetically favorable ($\Delta E < 0$) formation of the MDLs in SC-CSNPs with hemispherical cores of normalized radius $R_0/a = 0.2\ldots0.9$. The most favorable (optimal) position $z_{0,opt}$ of the MDL is clearly indicated by the minimum at the energy

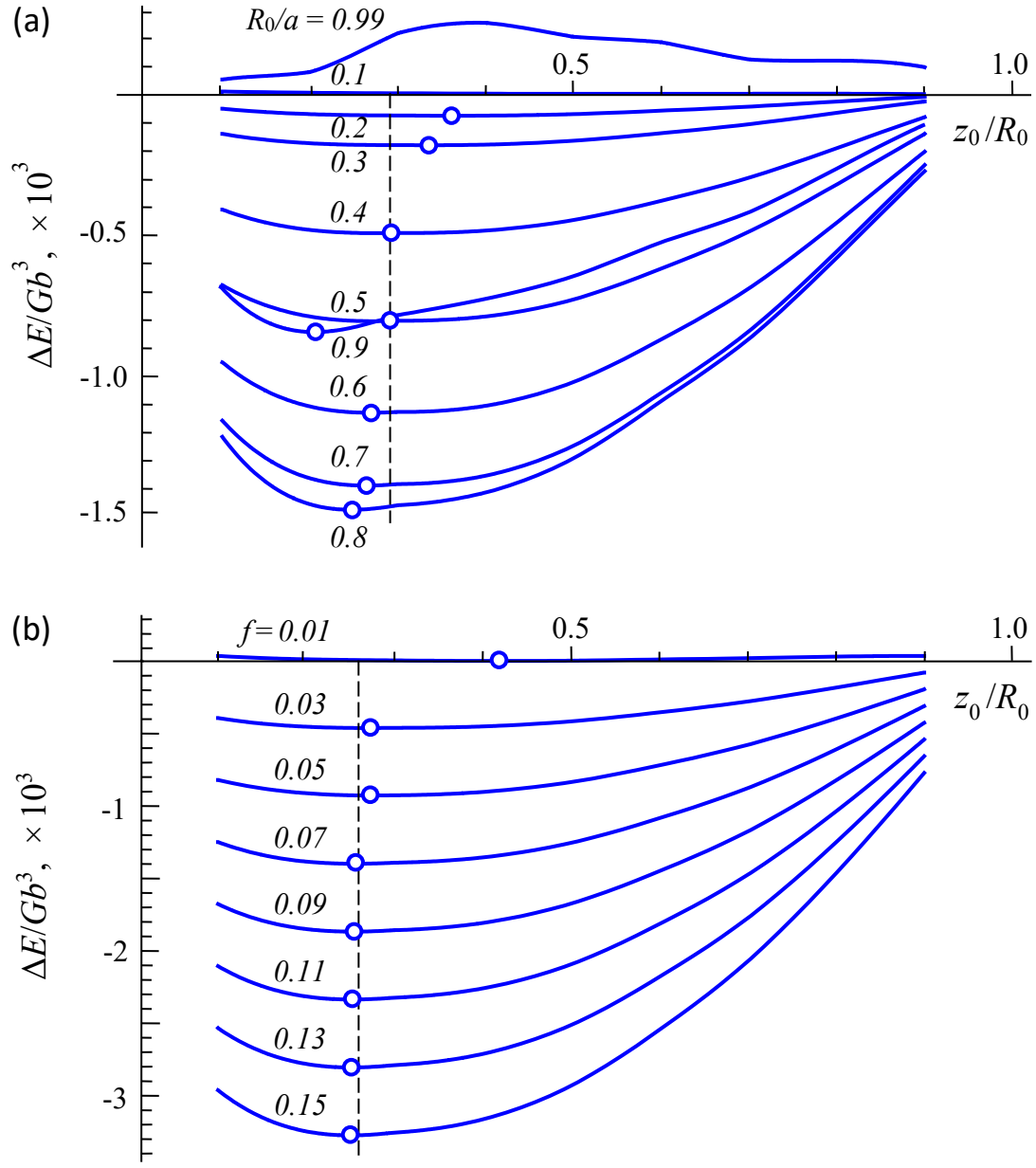

Fig. 12. Dependence of the energy change ΔE on the normalized coordinate of the MDL z_0/R_0 for (a) $f = 0.02$ and different values of the ratio R_0/a, and (b) $R_0/a = 0.3$ and different values of the misfit f. The small circles indicate the minima on the curves. Adopted from [40]

curves. For $R_0/a = 0.2$, it is $z_{0,opt} \approx 0.36R_0$; for $R_0/a = 0.3$, it is $z_{0,opt} \approx 0.33R_0$; for larger values of the ratio, $R_0/a = 0.4$ and 0.5, it remains approximately constant, $z_{0,opt} \approx 0.30R_0$; and then it slightly decreases again with R_0/a. Finally, at $R_0/a = 0.9$, it falls down to $z_{0,opt} \approx 0.20R_0$. For either very fine ($R_0/a = 0.1$) or very coarse ($R_0/a = 0.99$) cores, the MDL formation is not energetically favorable ($\Delta E \geq 0$). It was also noted in [40] that the energy gain $|\Delta E_{\min}|$, caused by the MDL generation, increases with the ratio R_0/a in its interval from 0.2 to 0.8 and then drastically drops at $R_0/a = 0.9$.

In the case, when $R_0/a = 0.3$ and f is varied from 0.01 to 0.15 (Fig. 12(b)), the misfit value $f = 0.01$ can be treated as the critical one for this value of the ratio R_0/a.

The corresponding curve has a minimum at $z_0/R_0 \approx 0.42$ where $\Delta E = 0$. At higher values of f (here from 0.03 to 0.15), $\Delta E < 0$ for any value of z_0/R_0. It is of interest that all these curves have minima approximately at the same point $z_0/R_0 \approx 0.26$. As it concluded in [40], for $R_0/a = 0.3$ and any $f \geq 0.02$ (see also Fig. 12(a)), the optimal position of the MDL is $z_{0,opt} \approx 0.26R_0$. It is also seen that the energy gain $|\Delta E_{\min}|$ monotonously increases with the misfit $f > f_c \approx 0.01$.

A detailed study of the optimal position $z_{0,opt}$ in dependence on the misfit f and the ratio R_0/a for $a = 200b$ and $\nu = 0.3$ (see Fig. 4 in [40]) showed that, for a wide range of the model parameters, $z_{0,opt}/R_0$ is close to 0.3. Then, taking $z_0/R_0 = 0.3$, the authors [40] considered the dependence of the energy change ΔE on the ratio R_0/a for different values of the misfit f in the interval from 0.001 to 0.030 (Fig. 13). The corresponding non-monotonous curves $\Delta E(R_0/a)$ may have one or two extremum points in dependence on f. When f is relatively small (here $f = 0.001$), the curve has a maximum (here at $R_0/a \approx 0.9$), and $\Delta E > 0$ for any value of R_0/a, which means that no MDL can form around the core. At a larger value of f (here at $f = 0.004$), the maximum shifts to the region of smaller R_0/a (here to the point $R_0/a \approx 0.46$), while a minimum appears on the curve (here at $R_0/a \approx 0.7$) , although $\Delta E > 0$ still always. Then, at a critical misfit value f_c (here $f_c = 0.0055$), the energy change ΔE becomes negative in the region of its minimum (here at $R_0/a \approx 0.74$) , which means that a MDL can form around the core in such a SC-CSNP. The positions of the maxima strongly depend on f, shifting to smaller values of R_0/a with increasing f, while the positions of the minima slightly shift to greater values of R_0/a, remaining however in the range from $R_0/a \approx 0.74$ to ≈ 0.78.

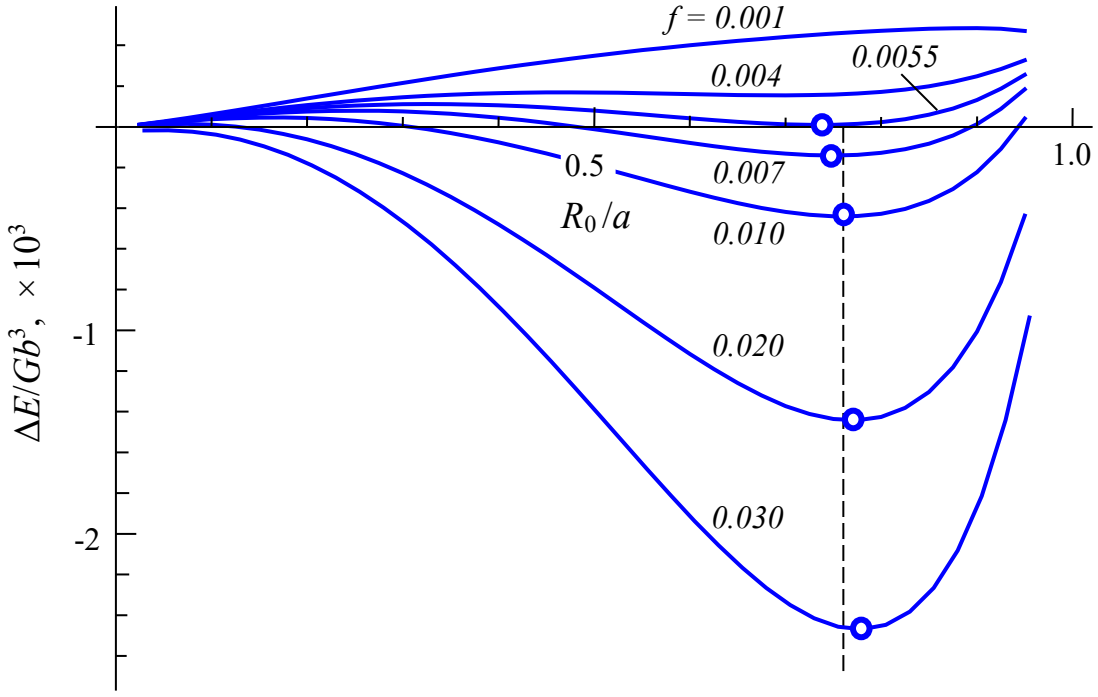

Fig. 13. Dependence of the energy change ΔE on the ratio R_0/a for the normalized position $z_0/R_0 = 0.3$ of the MDL and different values of the misfit strain f. Adopted from [40]

For $f > f_c$, there is an interval of R_0/a values, where $\Delta E < 0$, in which a MDL can form. Outside this interval, $\Delta E > 0$ and no MDL can nucleate. The boundaries of this interval can be considered as critical values of the ratio R_0/a, $(R_0/a)_{c1}$ and $(R_0/a)_{c2}$, for a given value of f. When f increases, $(R_0/a)_{c1}$ decreases, while $(R_0/a)_{c2}$ increases. These conclusions of [40] are rather similar to those obtained earlier for axially symmetric core-shell nanowires [46] and CSNPs with centered spherical cores [2,39,41,42].

When f is significantly larger then f_c (here at $f = 0.02$), the upper boundary $(R_0/a)_{c2}$ of the interval practically disappears, while its lower boundary $(R_0/a)_{c1}$ still exists. However, when $f >> f_c$ (here at $f = 0.03$), both the maximum on the curve $\Delta E(R_0/a)$ and the critical interval disappear, which means that a MDL can form for any value of R_0/a.

Since the point of minimum on the curve $\Delta E(R_0/a)$ remains almost the same, at $R_0/a \approx 0.76 \approx 3/4$ (Fig. 13), the authors [40] concluded that SC-CSNPs with the ratio $R_0/a \approx 3/4$ are the less stable to the MDL formation because in this case, the appearance of MDLs leads to the biggest energy gain $|\Delta E_{\min}|$ of the system. They also noted that their additional calculations showed that this result did not change for other values of the SC-CSNP radius a.

Figure 14 shows the diagrams $f_c(R_0/a)$ plotted in [40] for the SC-CSNPs with semispherical (solid red curves) and, for comparison, spherical (dashed blue curves) cores [39] for $z_0/R_0 = 0.3$ and different values of the normalized radius a/b of the SC-CSNP. The region under (above) the curve corresponds to the case when the MDL formation is not (is) energetically favorable. Similar diagrams were constructed and discussed in detail for different models describing the critical conditions of MD generation in the past [2,39,41,42,46] (see also Figs. 3(b), 5(b), 9, and 10 in the present review). In Fig. 14, the curves $f_c(R_0/a)$ for SC-CSNPs with semispherical cores lie above the corresponding curves for SC-CSNPs with spherical cores in the range of $R_0/a < 0.9$. It means that in this range, the SC-CSNPs with semispherical cores are more stable with respect to MDL generation than the SC-CSNPs with spherical cores. However, at $R_0/a \approx 0.9$, the curves for semispherical and spherical cores meet, which means that the SC-CSNPs with semispherical and spherical cores become equally stable (unstable) with respect to MDL generation. The authors [40] did not consider the range of $R_0/a > 0.9$ because the misfit stress fields [57] poorly converge near the free surface of the SC-CSNP.

It is worth noting that, for SC-CSNPs with semispherical cores, the formation of a straight MD at the core base along the diameter of a SC-CSNP was also considered [58]. In this case, the recently found solution of the boundary-value problem in the elasticity theory for a straight edge dislocation in an elastic sphere [59] was used. It was shown that for relatively small cores, the formation of a straight MD at the core base is less favorable than the formation of a circular MDL around the spherical part of the core/shell interface. However, for cores whose radii are close to the shell radius, both of these mechanisms are approximately equivalent. The authors [58] explained it by the facts that for small cores, the self-energy of a MDL is significantly less than for a straight dislocation intersecting a SC-CSNP, and on the other hand, for large cores, the elastic fields of the MDL are too strongly screened by the free surface, which significantly reduces the interaction energy of the MDL with the misfit stress field. Therefore, as the core radius tends to the shell radius, the formation of a MDL becomes less favorable than the formation of a straight MD.

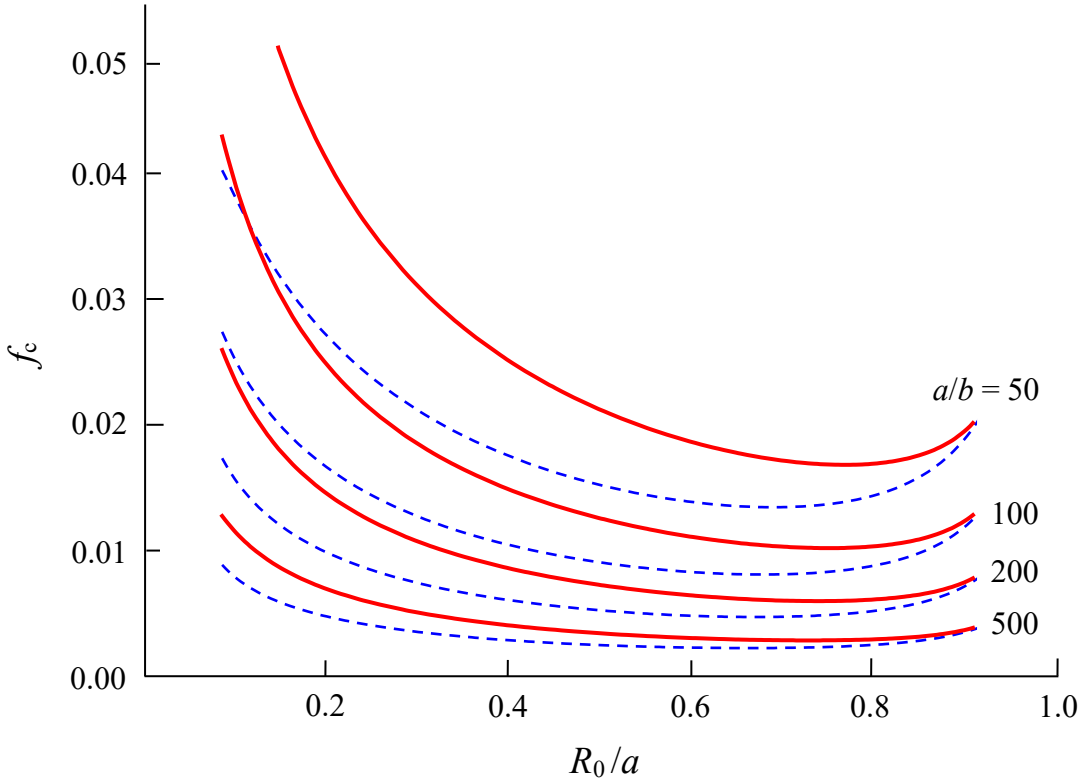

Fig. 14. Dependence of the critical misfit f_c on the ratio R_0/a for $z_0/R_0 = 0.3$, $\nu = 0.3$ and different values of the normalized radius a/b of the nanoparticle. The solid (red) curves show the solution for a semispherical core, while the dashed (blue) curves for a spherical core. Adopted from [40]

In all the aforementioned models, the critical conditions for the onset of already formed MDLs in CSNPs were analyzed. However, neither the physical processes of MDL nucleation and formation nor the energy barriers, which could accompany these processes, were considered. To overcome these drawbacks, the authors of [60] suggested a model of nucleation of an initial defect configuration capable to develop in a final configuration of the first closed MDL around the core. They assumed that the initial defect configuration could be a small PDL nucleating from either the inner or outer boundary in the SC-CSNP and propagating into its core or into its shell. The critical conditions for nucleation of such a PDL were calculated by using Eqs. (14) and (15) with appropriate formulas for the energy terms [60]. In particular, the approximation of the classical linear isotropic theory of elasticity was used with the assumptions that the core and the shell had identical elastic moduli and that the shell thickness *h* was substantially smaller than the outer radius of the SC-CSNP *R*: *h* << *R*. With the latter assumption, the authors [60] passed in calculation of the strain energy term from the spherical to planar geometry of the problem and considered a rectangular PDL. In this case, the solution for the strain energy of a rectangular PDL located in a plane perpendicular to the plane of the free surface of the elastic half-space [61] was used.

Thus, the authors [60] calculated the critical conditions for relaxation of misfit stresses in SC-CSNPs through the generation of rectangular PDLs at either the internal core-shell interface or the outer free surface with their subsequent propagation into the core or into the shell in the cases where the PDLs have the shape of a square or are

extended along or across the interface. As a result, they investigated the necessary conditions for the generation of PDLs of nine types classified according to the shape of the PDL and the position of its formation. It was shown that such PDLs can form when the misfit f exceeds a critical value that depends on R, h, the PDL formation position, and the shape of PDLs. For a PDL generating in the shell, this condition holds when h either lies in a specific range of small values or (for a larger value of f) is less than a critical value. For a PDL generating in the core, h should exceed a critical value. It was also shown that the PDLs elongated along the core-shell interface are formed easier. When the shell grows on the core of a fixed radius, the energetically more preferable generation of a PDL occurs first from the free surface into the bulk of the shell, then from the interface into the shell, and finally from the interface into the core of the SC-CSNP.

The model [60] of misfit stress relaxation through generation of rectangular PDLs in SC-CSNPs was later extended to various heterogeneous nanostructures. In particular, PDL generation in heteronanostructures of spherical (solid [62,63] and hollow [62–64] SC-CSNPs), infinite cylindrical (solid [63–67] and hollow [63,64] core-shell nanowires), flat (bi- and tri-nanolayers [63,64]), and finite-length tubular [68] geometry was analyzed. Departing from the calculations of the misfit stress fields in the heteronanostructures, the authors investigated changes in their energies caused by the formation of PDLs in different regions of them, revealed the regions of the energetically more preferable generation of the PDLs and specified the optimum shape of the PDLs. Gutkin and Smirnov [63,64] compared the critical conditions for the onset of the most energetically favorable PDLs in different heteronanostructures and ranged the relative stabilities of these nanostructures against PDL formation. They concluded hollow nanostructures are always more stable than their solid counterparts, the cylindrical nanostructures are more stable than the symmetric flat tri-nanolayers, the spherical nanostructures are more stable than the cylindrical ones, and the flat bi-nanolayers are the most stable nanostructures among those under consideration.

Critical conditions for misfit dislocation generation in composite nanowires

Critical conditions for MD generation in composite nanowires of different architectures have remained in the focus of many authors for a long time (see, for example, books [11–13] and reviews [22–27,69]). The main segments in this field are theoretical models for: straight MDs [46,70–74], circular [30,70,75–80] and elliptic [81] MDLs, and rectangular PDLs [63,64] in core-shell nanowires (CSNWs) with cylindrical cores; straight MDs [82] and rectangular PDLs [65–67] in CSNWs with prismatic cores of hexagonal, squared and triangular cross section; straight MDs [47,83,84], circular MDLs [32] and rectangular PDLs [63,64] at/in nanotubes embedded to infinite matrix; straight MDs [85–87] and circular PDLs [88] in axially-inhomogeneous nanowires with transverse interfaces; straight MDs in bilayer nanowires with planar interfaces [89–93]; circular MDLs around axially symmetric finite-length cylindrical inclusions in nanowires [28].

Since the most of these models have been extendedly reviewed in recent years [24–27,69], here we briefly consider only some fresh results [91–93] which have been reported in conference talks but not published in regular journals yet.

Figure 15 shows a model [91] of the cross-section of a bilayer nanowire with a flat longitudinal interface in the initial coherent and partly relaxed states. The nanowire was supposed elastically isotropic and homogeneous. The initial coherent state in this case is different from those considered in earlier models [89,90] where the one-dimensional lattice misfit along the x-axis was assumed and modeled through a continuous distribution of virtual edge dislocations with infinitesimal Burgers vectors $\delta\mathbf{b} = \delta b\mathbf{e}_x$ (here δb is the infinitesimal Burgers vector magnitude and $\mathbf{e}_x$ is the ort of the x-axis). In models [91–93], the authors considered the general case of three-dimensional lattice misfit $f = 2(a_2 - a_1)/(a_2 + a_1)$ and solved the corresponding boundary-value problem in the classical theory of elasticity.

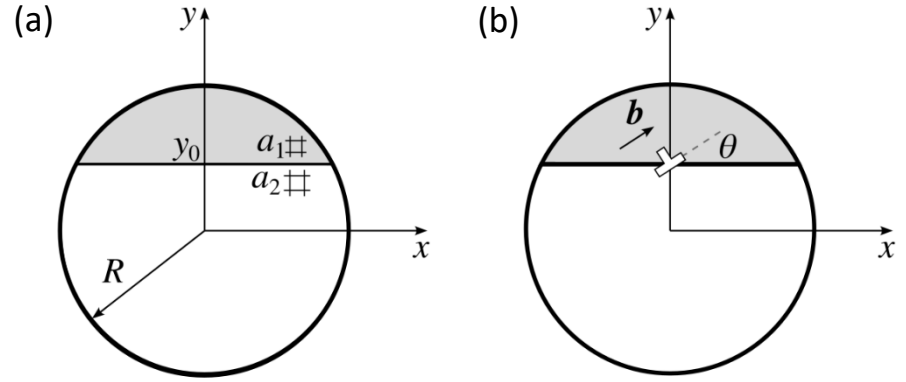

Fig. 15. Cross-section of a bilayer nanowire in (a) the initial coherent state and (b) the partly relaxed state with a misfit dislocation. Here a_1 and a_2 are the lattice parameters in the nanowire layers, R is the nanowire radius, $y = y_0$ is the interface position, $\boldsymbol{b}$ is the Burgers vector of the misfit dislocation, and ϑ is the angle between the Burgers vector and the interface plane. Adopted from [91]

The onset of the first straight edge MD at the interface (Fig. 15(b)) needs the fulfillment of the common inequality $\Delta W = W_{\mathrm{el}} + W_{\mathrm{c}} + W_{\mathrm{int}}$, where ΔW is the energy change caused by the generation of the MD, W_{el} is the MD strain energy, W_{c} is its core energy, and W_{int} is the energy of interaction of the MD with the initial misfit stress in the nanowire. All these energy terms are calculated per unit length of the MD. Then the critical misfit follows from the equation $\Delta W = 0$ as [91]:

$$f_{\mathrm{c}} = \frac{3g(t)}{8(1+\nu)s\cos\theta}\left(\ln\alpha\, s + \ln(1-t^2) + t^2\cos^2\theta - \frac{3-4\nu}{4(1-\nu)}\right), \tag{23}$$

where $s = R/b$, $t = y_0/R$, α is the dislocation core energy parameter [38], ν is the Poisson ratio, and $g(t)$ is the dimensionless function equal to 1 for $t = 0$ and given by:

$$g(t) = \frac{2t^3}{3(1-t^4)(\arcsin t - t\sqrt{1-t^2})}, \text{ for } 0 < |t| < 1. \tag{24}$$

Figure 16 shows the dependence of the critical misfit f_{c} on the normalized position t of the interface for different values of radius R at $\nu = 0.3$, $\alpha = e$ (here e is the base of natural logarithm), and $\theta = 30°$. As is seen, the critical misfit f_{c} depends on both the nanowire radius R and interface position y_0. It increases with a decrease in R and behaves non-monotonously with an increase in y_0: f_{c} slowly decreases with y_0 at relatively small values of y_0, reaches its minimum value $f_{\mathrm{c,min}}$ at some intermediate value of y_0 varying from roughly $0.48R$ in the range of relatively large values of R (here for $R \geq 50b$) to roughly $(0.50–0.54)R$ at smaller values of R (here at $R = 25b$ and $10b$), and then increases

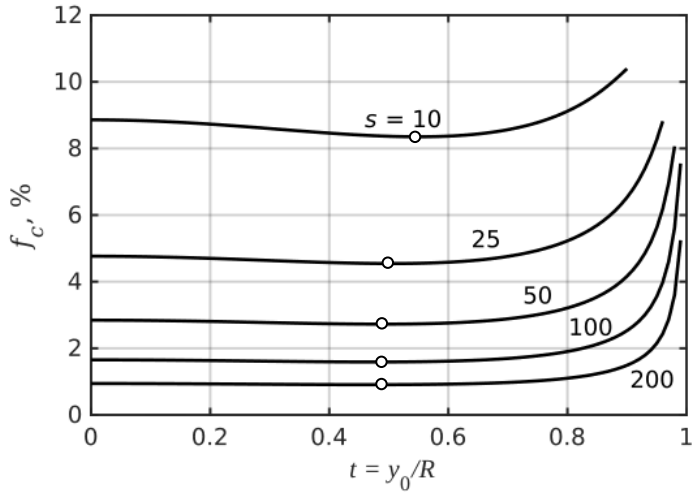

Fig. 16. Dependence of the critical misfit f_c on the normalized position t of the interface for different values of the normalized radius $s = R/b$ at $\nu = 0.3$, $\alpha = e$, and $\theta = 30°$. The open dots indicate the minima of the curves. Adopted from [91]

with y_0, especially fast when $y_0 \geq 0.8R$. Thus, it was shown in [91] that bilayer nanowires with asymmetric position $y_0 \approx R/2$ of the interface are the most unstable with respect to MD generation.

The misfit stress relaxation in the same model system (Fig. 15(a)) through the formation of equilibrium discrete ensembles of edge MDs was considered in [92]. The number and arrangement of MDs were chosen to minimize the energy W of the system per unit area of the interface. As a result, the dependence of this energy W on the misfit f was studied for $R = h$ and $2h$, where $h = R - y_0$ is the maximum thickness of the 'upper' layer, and compared with that for a thin flat epilayer of thickness h on a thick substrate (Fig. 17). It is seen that, for a given value of h, the misfit relaxation with increasing f in the nanowire begins expectedly later than, for example, in a thin flat epilayer on a thick substrate. On the other hand, it was also shown [92] that, at a sufficiently high level of f (here for f > 20 %) the density of the MD ensemble is practically independent on the configuration of the system.

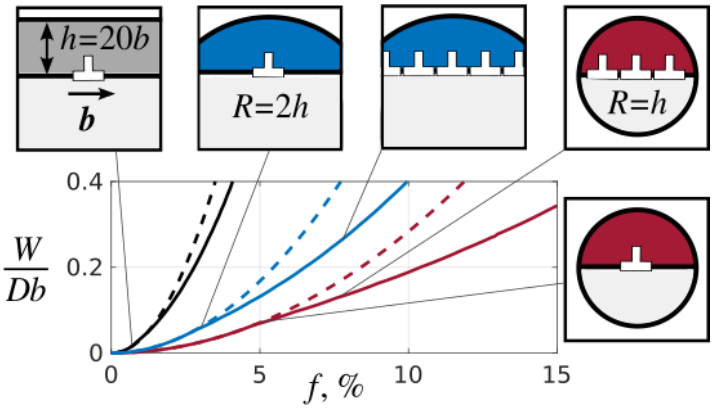

Fig. 17. Dependence of the energy W on the misfit f for $h = 20b$. Here $D = G/[2\pi(1-\nu)]$, G is the shear modulus, ν is the Poisson ratio, and b is the Burgers vector magnitude of the misfit dislocations. The dashed curves show similar dependences for the corresponding systems in the coherent state (with no MDs). Adopted from [92]

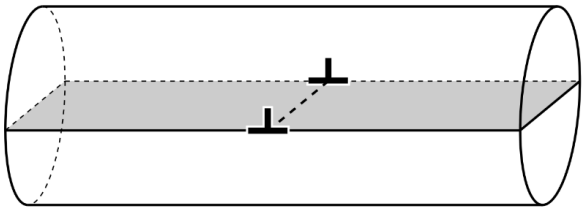

Fig. 18. A straight edge MD piercing a symmetrical bilayer nanowire normally to its axis. Based on results given in [93]

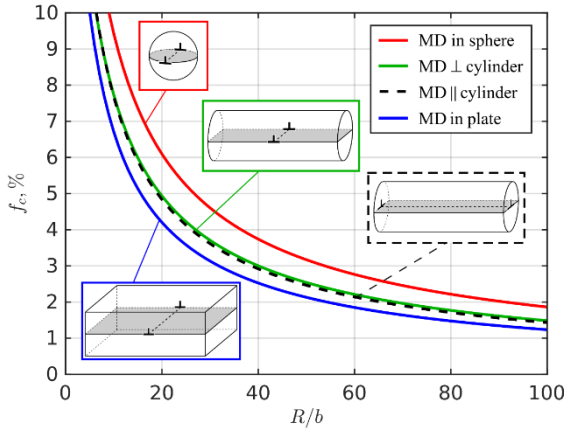

Fig. 19. Dependence of the critical misfit f_c for the formation of straight edge MDs in different Janus nanostructures – a symmetrical bilayer cylinder of radius R, a sphere of radius R and a plate of thickness $2R$ – on their normalized characteristic size R/b at $\nu = 0.3$ and $\alpha = e$. Based on results given in [93]

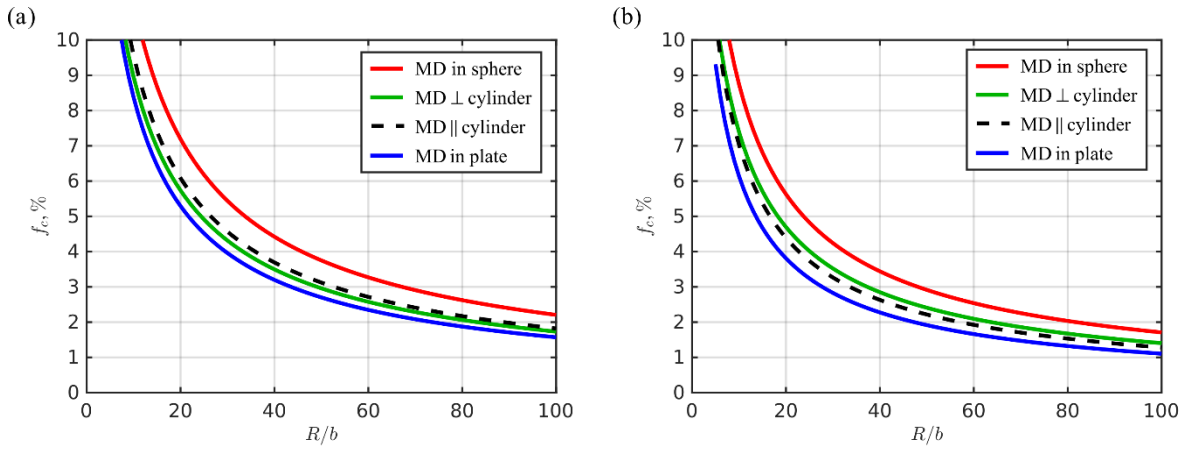

Fig. 20. Dependence of the critical misfit f_c for the formation of straight edge MDs in different Janus nanostructures – a symmetrical bilayer cylinder of radius R, a sphere of radius R and a plate of thickness $2R$ – on their normalized characteristic size R/b at $\alpha = e$ and (a) $\nu = 0$ and (b) $\nu = 0.49$. Based on results given in [93]

MD lines in models [89–92] were parallel to the nanowire axes. Obviously, it would be also reasonable to consider the nonparallel case. However, modeling of such configurations is hindered by the lack of analytical solutions for the boundary-value elastic problems on cylinders with straight dislocations piercing the free surface of the cylinders. Thus, calculating the dislocation strain energy W_{el} becomes a matter of numerical approximations. On the other hand, the interaction energy W_{int} can still be obtained

analytically with the aforementioned solution for the misfit stress-field of a bilayer nanowire [92]. In such a manner, the misfit stress relaxation in a symmetrical bilayer cylinder via the formation of an edge MD perpendicular to the cylinder axis (Fig. 18) was considered in [93]. The strain energy W_{el} was calculated with the finite element method and verified by comparison with several well-known analytical solutions for other systems. The results show that the values for the critical misfit f_c for both the parallel and perpendicular MDs in a symmetrical bilayer cylinder are rather close (Fig. 19). However, it is of interest that the exact relation between those two cases depends on the Poisson ratio ν (Fig. 20): for $\nu = 0$, the perpendicular MD is more preferable than the parallel one, while for $\nu = 0.49$ it is vice versa, and for intermediate values (here for $\nu \approx 0.3$, see Fig. 19), the critical misfits are practically equal. In any case, both the critical misfits for a bilayer cylinder of radius R lie between the critical misfit values for a symmetrical bilayer plate of thickness $2R$ and a Janus sphere of radius R. Thus, comparing different architectures of Janus nanostructures, one can conclude that the Janus plate is less stable to the MD generation than the Janus cylinder, while the latter is less stable in this respect than the Janus sphere. This result well corresponds to the earlier comparison of the stability of different misfitting nanostructures to the formation of small rectangular PDLs [63,64].

Theoretical models for misfit dislocations in free-standing composite nanolayers

The theoretical models describing the elastic fields and strain energy of MDs, and critical conditions for their generation in free-standing composite nanolayers were suggested and studied by a number of authors. In particular, they considered: straight edge MDs in misfitting bi- [44,94–102], tri- [102,103], and multilayers [94] with two free surfaces and either different [44,94–96,99–102] or equal [96,98,103] elastic constants, isotropic [44,94–98,103] and anisotropic [99–102]; a periodic set of straight screw interfacial MDs normally piercing the free surfaces of a plate-like heterogeneous bicrystal with different isotropic elastic moduli [104,105]; dipoles of straight edge MDs in the interfaces of a lamellar inclusion piercing a nanolayer normally to its free surfaces [106,107]; a circular MDL in the interface of a circular cylindrical inclusion piercing a nanolayer normally to its free surfaces [108]; straight edge MDs in a nanolayer with an embedded nanowire of rectangular cross section with the faces parallel and normal to the nanolayer free surfaces [109]. It is worth noting that model nanostructures in works [106–109] were assumed elastically isotropic and homogeneous.

Some of the authors concentrated their attention on the calculation of elastic fields of some presumed periodic configurations of MDs at the interfaces [94,95,97,99,100,104,105], while the others also analyzed the energetics of partly relaxed nanolayers with MDs [44,96,98,101–103,106–109], the critical conditions for the onset of MD generation process [44,96,103,106–109], and the energy barriers for its realization [103,109]. The discussion of the critical conditions was based on the calculation of the energy changes accompanied the MD appearance in the misfitting nanolayers as was also the case with composite nanoparticles and nanowires (see the previous sections). The differences were in the self-strained energies of MDs and the energies of their interaction with the initial misfit stresses that were found according to the geometry of the nanolayers under study. Moreover, the earlier models [44,94–100] were already reviewed in book [11]. To avoid

repeating, here we consider in more details only the most recent models [103,109] dealing with analyzing possible mechanism of MD generation with corresponding critical conditions and energy barriers.

Mikaelyan et al. [109] suggested a model of misfit stress relaxation in and around a nanowire of rectangular cross section embedded in a nanolayer in such a way that opposite faces of the nanowire are parallel or normal to the nanolayer surfaces (Fig. 21). Within the model, an edge of the nanowire, which is closer to the nanolayer surface, emits a dipole of edge dislocations, either perfect or partial, which glide along the nanowire face normal to the free surfaces of the nanolayer. One of these dislocations glides from the nanowire edge to the free surface, while the other one glides to the middle of the nanowire face. Based on the earlier solutions of the boundary-value problems in the theory of elasticity for a rectangular dilatational inclusion in a thin layer [110] and for an edge dislocation in a thin two-layer plate [111], the authors calculated the total energy change ΔW caused by the dislocation emission and analyzed it with the help of energy maps built in coordinates of emitted dislocations x_1 and x_2.

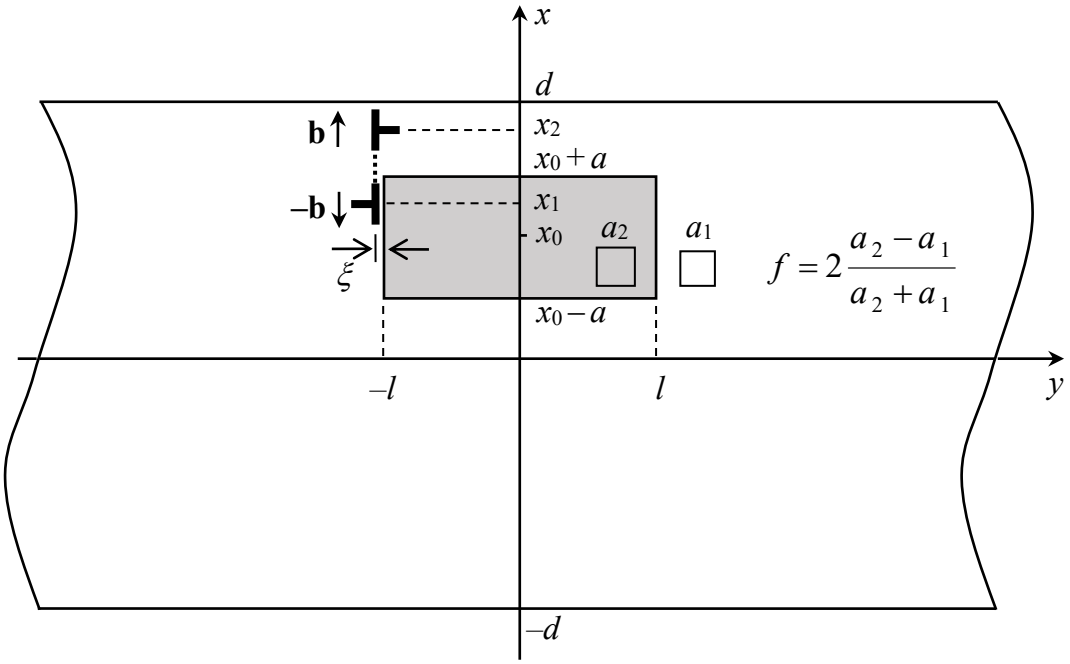

Fig. 21. Misfit stress relaxation near a nanowire having a rectangular cross section with sizes $2l \times 2a$, embedded in a nanolayer of thickness $2d$, through the emission of a dipole of edge dislocations with Burgers vectors $\pm\boldsymbol{b}$ from one of two nanowire edges which are closer to the free surface of the nanolayer. Adopted from [109]

Figure 22 shows some examples of these energy maps $\Delta W(x_1, x_2)$ plotted for a model nanostructure of a Ge nanowire embedded in a Si nanolayer with the following set of the material parameters: the misfit value $f = 0.042$, the shear modulus $G = 60$ GPa, the Poisson ratio $\nu = 0.26$ and the stacking fault energy $\gamma_{SF} = 0.069$ Jm^{-2} (for the case of emission of partial dislocations). The Burgers vector magnitudes for partial and perfect dislocations were $b = 0.23$ and 0.46 nm, respectively. For the sake of definiteness, the authors [109] fixed the position of the nanowire center in the nanolayer as $x_0 = 25$ nm.

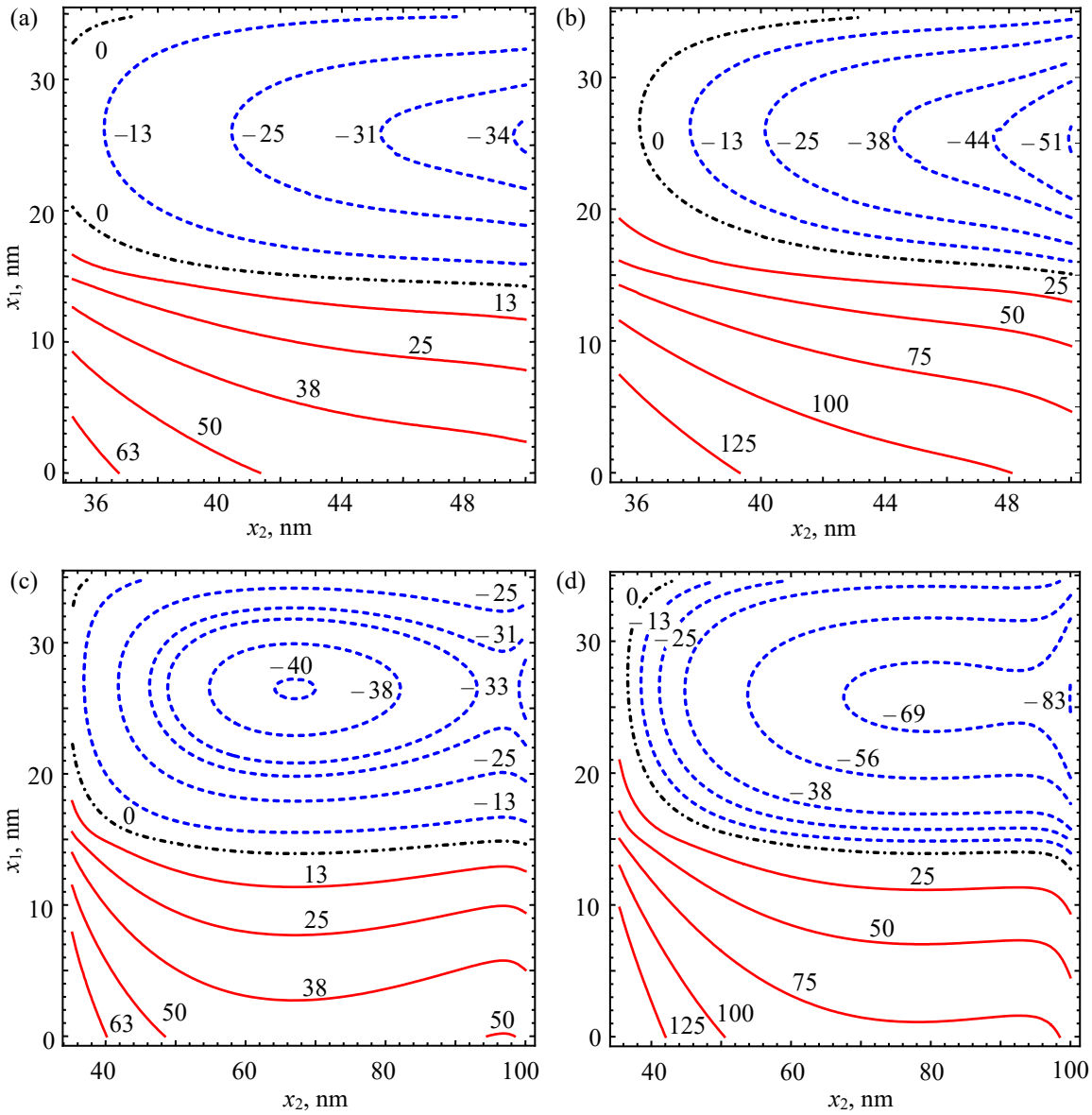

Fig. 22. The maps of the energy change $\Delta W(x_1, x_2)$ in the coordinates of emitted dislocations for the model nanostructure of a Ge nanowire embedded in a Si nanolayer for (a, c) partial and (b, d) perfect dislocations at $x_0 = 25$ nm, $2a = 20$ nm, $2l = 50$ nm, and $2d = 100$ nm (a, b) and 200 nm (c, d). The energy values are given in eV/nm. Adopted from [109]

They also assumed that the crystalline lattices of the nanowire and nanolayer materials were oriented in such a manner that the glide plane of the dislocations was of {111}-type, that is the plane of easy slip for partial (Shockley) dislocations.

With these assumptions, the authors [109] chose the sizes of the nanowire cross section as $2l = 50$ nm and $2a = 20$ nm and plotted the energy maps $\Delta W(x_1, x_2)$ for partial (Fig. 22(a,c)) and perfect (Fig. 22(b,d)) dislocations for two typical values of the nanolayer thickness $2d = 100$ nm (Fig. 22(a,b)) and 200 nm (Fig. 22(c,d)). The starting points of dislocation emission were assumed to be $x_{10} = x_0 + a - b = (35 - b)$ nm and $x_{20} = x_0 + a + b = (35 + b)$ nm, so after emission the coordinate x_1 decreased, while the coordinate x_2 increased. In a map, these starting points give a point $(x_{10}, x_{20}) = (35 - b, 35 + b)$ which lies near the top left corner of the map. As is seen, this point is situated in the region

of positive values of ΔW, and the value of $\Delta W(x_{10}, x_{20})$ may be considered as an energy barrier W_{em} for dislocation emission. The calculations showed [109] that for partial dislocations, W_{em} is about 2.8 eV/nm for $2d = 100$ nm and 3.0 eV/nm for $2d = 200$ nm; for perfect dislocations, W_{em} is about 13.1 eV/nm for $2d = 100$ nm and 13.4 eV/nm for $2d = 200$ nm. Thus, the authors [109] concluded that the energy barrier strongly depends on the type of emitted dislocations but weakly depends on the nanolayer thickness. On the other hand, they also showed that W_{em} weakly depends on the nanowire size.

Figure 23 shows the dependence of W_{em} on d for two different values of $2l$, $2l = 10$ and 50 nm, at $2a = 20$ nm. As is seen from Fig. 23, W_{em} increases with a decrease in the nanowire size. This is so because the misfit shear stress at the points of dislocation emission increases with the nanowire size [112]. The authors [109] concluded that, in general, the nucleation of partial dislocations is much more probable than that of perfect dislocations in this model system of Ge nanowire in Si nanolayer. In particular, at $W_{em} \approx 3$ eV/nm, the partial dislocations can be emitted even at room temperature in this system. In contrast, the emission of perfect dislocations with $W_{em} \approx 13$ eV/nm is possible only at much higher temperatures.

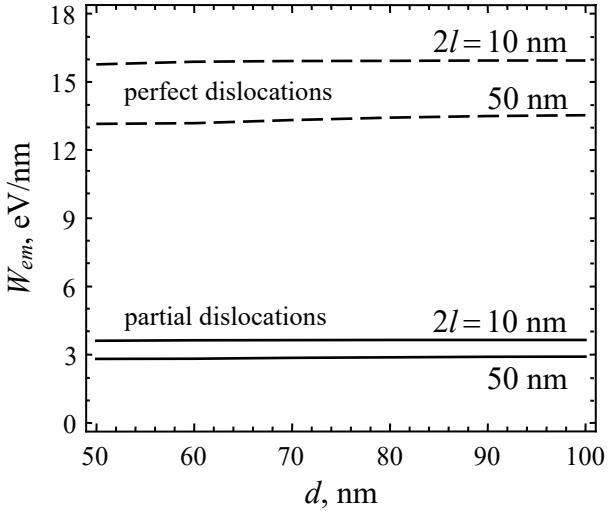

Fig. 23. Dependence of the energy barrier W_{em} on the nanolayer half-thickness d for partial and perfect dislocations at the following values of the system parameters: $x_0 = 25$ nm, $2a = 20$ nm, and $2l = 10$ and 50 nm. Adopted from [109]

It is evident from the energy maps in Fig. 22 that if the dislocation dipole nucleate, the dislocations start to feel at once driving thermodynamic forces which stimulate their glide to the opposite directions. In a map, their motion is reflected by the trajectory which follows the maximum gradient of the function $\Delta W(x_1, x_2)$ and tends to the minimum of this function. In the case of partial dislocations, this minimum can be localized either on the right margin of the map (Fig. 22(a)) or in its central region (Fig. 22(c)). The first situation is characteristic for a relatively thin nanolayer (here with the thickness $2d = 100$ nm) when one dislocation (with coordinate x_1; the authors [109] called it x_1-dislocation) reaches its stable equilibrium position $x_{1eq} \approx 26$ nm at the middle of the nanowire face, while the other dislocation (with coordinate x_2; the authors [109] called it x_2-dislocation) achieves its stable equilibrium position $x_{2eq} = 50$ nm on the free

surface of the nanolayer. The second situation is characteristic for a relatively thick nanolayer ($2d = 200$ nm) when the x_1-dislocation also reaches its stable equilibrium position $x_{1eq} \approx 26$ nm at the middle of the nanowire face, while the x_2-dislocation stops inside the nanolayer, at the stable equilibrium position $x_{2eq} = 67$ nm.

In the case of perfect dislocations, the minimum of function $\Delta W(x_1, x_2)$ was always localized on the right margin of the map (Figs. 22(b,d)). As follows from its position, the x_1-dislocation reaches its stable equilibrium position $x_{1eq} \approx 25$ nm at the middle of the nanowire face, while the x_2-dislocation glides to its stable equilibrium positions $x_{2eq} = 50$ nm (for $2d = 100$ nm) and 100 nm (for $2d = 200$ nm) on the free surface of the nanolayer.

Thus, the calculations of [109] show that perfect dislocations (if they can overcome the energy barrier for their nucleation) must occupy two stable equilibrium positions, one in the middle of the nanowire face and the other one on the free surface of the nanolayer. This situation does not depend on the nanowire and nanolayer sizes. In the case of partial dislocations, whose nucleation is much more probable than that of perfect ones, one dislocation must always occupy its stable equilibrium position at the middle of the nanowire face, while the equilibrium position of the second dislocation depends on the nanowire and nanolayer sizes.

Colin [103] considered a model of misfit strain relaxation in a three-layer structure through the climb of one and two straight edge dislocations from the 'upper' free surface (Fig. 24). He calculated the equilibrium positions of the dislocations, the energy barriers for their climb to the interface, and the critical misfit values for their generation under the assumptions that the second dislocation climbs in the same path as the first one and that the effects of the 'lower' free surface on the dislocation stresses can be neglected.

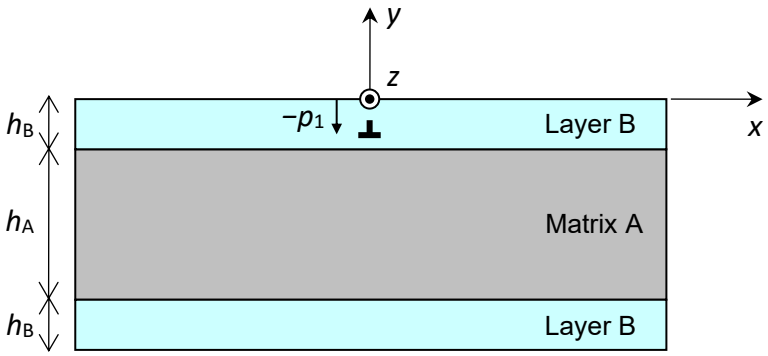

Fig. 24. Two layers of material B and thickness h_B cover a matrix of material A and thickness h_A. An edge dislocation with Burgers vector **b** = (b, 0) lies at a position (0,$-p_1$) in the upper layer. Adapted from [103]

Conclusions

In general, it is shown that both classical and novel methods of the theory of spatial elasticity in combination with the micromechanics of defects form an effective approach which allows adequate description of the relaxation of misfit stresses in various inhomogeneous crystalline nanostructures – composite nanoparticles, nanowires and nanolayers. In recent decades, many new theoretical models have been elaborated within this approach. Significant progress has been achieved in describing the dislocation

mechanisms, the energy barriers, and the critical conditions of misfit stress relaxation in newly considered misfitting nanostructures such as solid and hollow core-shell nanoparticles and nanowires, core-shell nanowires with faceted cores, Janus nanoparticles and nanowires, spherical nanoparticles with semispherical cores, axially-inhomogeneous nanowires with planar transverse interfaces, embedded nanotubes, and free-standing nanolayers with embedded nanowires. Based on these achievements, one can conclude that the relative stability of different misfitting nanostructures to stress relaxation through generation of MDs increases with a decrease in the dimension of the nanostructures having the same characteristic sizes: the planar nanolayers (quasi 2D-nanostructures) are less stable than the cylindrical ones (quasi 1D-nanostructures), and the latter are less stable than the spherical ones (quasi 0D-nanostructures). Generation of partial MDs needs lower energy barriers to overcome than that of perfect MDs, although perfect MDs provide more effective relaxation of misfit stresses than partial MDs.

Among the problems of special interest in the nearest future, the following research areas can be noted:

1. further development of theoretical models of misfit stress relaxation in already analyzed nanostructures with special attention to the calculation of energy barriers for MD formation and equilibrium densities of MDs belonging to different families (for example, straight MDs and MDLs in core-shell nanowires);
2. comparative studying (when suitable and possible) the models for generation of partial and perfect MDs in various misfitting nanostructures;
3. invention of effective approaches for analytical modeling the misfit stress relaxation in faceted core-shell nanowires and nanoparticles;
4. formulation and solution of new boundary-value problems in the theory of elasticity for straight dislocations and disclinations shifted from the axial position in bulk, hollow and inhomogeneous spheres;
5. solution of new boundary-value problems in the theory of elasticity to determine misfit stress fields in inhomogeneous crystalline nanostructures with diffuse interfaces;
6. development of theoretical models for misfit stress relaxation in inhomogeneous crystalline nanostructures with diffuse interfaces.

It is expected that any progress in dealing with these problems will allow to obtain new results that will be useful for better understanding the behavior of defects, stress relaxation and related phenomena in real device nanostructures.

CRediT authorship contribution statement

Mikhail Yu. Gutkin: writing – review & editing, writing – original draft; **Anna L. Kolesnikova**: conceptualization; **Stanislav A. Krasnitckii**: data curation; **Kristina N. Mikaelyan**: data curation; **Dmitrii A. Petrov**: data curation; **Alexey E. Romanov**: supervision; **Andrei M. Smirnov**: writing – review & editing.

Conflict of interest

The authors declare that they have no conflict of interest.

References

1. Trusov LI, Tanakov MYu, Gryaznov VG, Kaprelov AM, Romanov AE. Relaxation of elastic stresses in overlayed microcrystals. *J. Cryst. Growth.* 1991;114(1–2): 133–140.
2. Gutkin MYu. Misfit stress relaxation in composite nanoparticles. *Intern. J. Eng. Sci.* 2012;61: 59–74.
3. Sneed BT, Young AP, Tsung CK. Building up strain in colloidal metal nanoparticle catalysts. *Nanoscale.* 2015;7(29): 12248.
4. Zhang Y, Wu J, Aagesen M, Liu H. III–V nanowires and nanowire optoelectronic devices. *J. Phys. D: Appl. Phys.* 2015;48(46): 463001.
5. Zhao J, Chen B, Wang F. Shedding light on the role of misfit strain in controlling core-shell nanocrystals. *Adv. Mater.* 2020;32(46): 2004142.
6. Frank FC, Van der Merwe J.H. One-dimensional dislocations. I. Static theory. *Proc. Roy. Soc. London A.* 1949;198(1053): 205–225.
7. Matthews JW. Defects associated with the accommodation of misfit between crystals. *J. Vac. Sci. Technol.* 1975;12(1): 126–133.
8. Tkhorik YuA, Khazan LS. *Plastic Deformation and Misfit Dislocations in Heteroepitaxial Systems*. Kiev: Naukova Dumka; 1983. (In Russian)
9. Milvidskii MG, Osvenskii VB. *Structural Defects in Epitaxial Layers of Semiconductors*. Moscow: Metallurgia; 1985. (In Russian)
10. Freund LB, Suresh S. *Thin Film Materials. Stress. Defect Formation and Surface Evolution*. Cambridge: Cambridge University Press; 2003.
11. Gutkin MYu, Ovid'ko IA. *Physical Mechanics of Deformed Nanostructures. Vol. II. Nanolayered Structures*. Saint-Petersburg: Yanus; 2005. (In Russian)
12. Gutkin MYu. *Strength and Plasticity of Nanocomposites: Textbook*. Saint-Petersburg: Izdatel'stvo Politekhnicheskogo universiteta; 2011. (In Russian)
13. Ovid'ko IA, Sheinerman AG. *Mechanics of Nanowires and Nanostructured Films*. Saint-Petersburg: Exlibris-Nord; 2011. (In Russian)
14. Matthews JW, Blakeslee AE. Defects in epitaxial multilayers: I. Misfit dislocations. *J. Cryst. Growth.* 1974;27: 118–125.
15. Matthews JW, Blakeslee AE. Defects in epitaxial multilayers: II. Dislocation pile-ups, threading dislocations, slip lines and cracks. *J. Cryst. Growth.* 1975;29(3): 273–280.
16. Matthews JW, Blakeslee AE. Defects in epitaxial multilayers: III. Preparation of almost perfect multilayers. *J. Cryst. Growth.* 1976;32(2): 265–273.
17. Van der Merwe JH. The role of lattice misfit in epitaxy. *CRC Crit. Rev. Sol. State Mater. Sci.* 1978;7(3): 209–231.
18. Schwartzman AF, Sinclair R. Metastable and equilibrium defect structure of II-VI/GaAs interfaces. *J. Electron. Mater.* 1991;20: 805–814.
19. Gutkin MYu, Kolesnikova AL, Romanov AE. Misfit dislocations and other defects in thin films. *Mater. Sci. Eng. A.* 1993;164(1–2): 433–437.
20. Beanland R, Dunstan DJ, Goodhew PJ. Plastic relaxation and relaxed buffer layers for semiconductor epitaxy. *Adv. Phys.* 1996;45(2): 87–146.
21. Jain SC, Harker AH, Cowley RA. Misfit strain and misfit dislocations in lattice mismatched epitaxial layers and other systems. *Philos. Mag. A.* 1997;75(6): 1461–1515.
22. Ovid'ko IA, Sheinerman AG. Misfit dislocations in nanocomposites with quantum dots, nanowires and their ensembles. *Adv. Phys.* 2006;55(7–8): 627–689.
23. Kavanagh KL. Misfit dislocations in nanowire heterostructures. *Semicond. Sci. Technol.* 2010;25(2): 024006.
24. Glas F. Strain in nanowires and nanowire heterostructures. *Semicond. Semimet.* 2015;93: 79–123.
25. Gutkin MYu, Kolesnikova AL, Romanov AE. Nanomechanics of stress relaxation in composite low-dimensional structures. In: Altenbach H, Öchsner A. (eds.) *Encyclopedia of Continuum Mechanics*. Berlin: Springer; 2020. p.1778–1799.
26. Smirnov AM, Krasnitckii SA, Rochas SS, Gutkin MYu. Critical conditions of dislocation generation in core-shell nanowires: A review. *Rev. Adv. Mater. Technol.* 2020;2(3): 19–43.
27. Romanov AE, Kolesnikova AL, Gutkin MY. Internal stresses and structural defects in nanowires. *Mech. Solids.* 2022;57(8): 1987–2004.
28. Gutkin MYu, Kuzmin KV, Sheinerman AG. Misfit stresses and relaxation mechanisms in a nanowire containing a coaxial cylindrical inclusion of finite length. *Phys. Stat. Sol. B.* 2011; 248(7): 1651–1657.
29. Kolesnikova AL, Gutkin MYu, Krasnitckii SA, Romanov AE. Circular prismatic dislocation loops in elastic bodies with spherical free surfaces. *Intern. J. Sol. Struct.* 2013;50(10): 1839–1857.

30. Chernakov AP, Kolesnikova AL, Gutkin MYu, Romanov AE. Periodic array of misfit dislocation loops and stress relaxation in core-shell nanowires. *Intern. J. Eng. Sci.* 2020;156(10): 103367.
31. Krasnitckii SA, Smirnov AM, Gutkin MYu. Pair interaction of coaxial circular prismatic dislocation loops in elastic solids with spherical surfaces. *Materials Physics and Mechanics*. 2020;44(1): 116–124.
32. Kolesnikova AL, Chernakov AP, Gutkin MYu, Romanov AE. Prismatic dislocation loops in crystalline materials with empty and coated channels. *Europ. J. Mech. – A/Solids.* 2022;94(10): 104612.
33. Lurie AI. *Spatial Problems of Theory of Elasticity*. Moscow: State Publishing House of Scientific and Technical Literature; 1955. (In Russian)
34. Prudnikov AP, Brychkov YuA, Marichev OI. *Integrals and Series. Special Functions*. Moscow: Nauka; 1983. (In Russian).
35. Dundurs J, Salamon NJ. Circular prismatic dislocation loop in a two-phase material. *Phys. Stat. Sol. B.* 1972;50: 125–133.
36. Kolesnikova AL, Romanov AE. *Circular dislocation-disclination loops and their application to boundary problem solution in the theory of defects*. Leningrad: Preprint No. 1019, Ioffe Physico-Technical Institute; 1986. (In Russian).
37. Eason G, Noble B, Sneddon IN. On certain integrals of Lipschitz-Hankel type involving products of Bessel functions. *Philos. Trans. Roy. Soc. Lond. A.* 1955;247: 529–551.
38. Hirth JP, Lothe J. *Theory of Dislocations*. New York: John Wiley & Sons; 1982.
39. Gutkin MYu, Kolesnikova AL, Krasnitckii SA, Romanov AE. Misfit dislocation loops in composite core-shell nanoparticles. *Phys. Solid State.* 2014;56(4): 723–730.
40. Gutkin MYu, Kolesnikova AL, Mikheev DS, Romanov AE. Misfit stresses and their relaxation by misfit dislocation loops in core-shell nanoparticles with truncated spherical cores. *Europ. J. Mech. / A Solids*. 2020;81: 103967.
41. Gutkin MYu, Kolesnikova AL, Krasnitckii SA, Romanov AE, Shalkovskii AG. Misfit dislocation loops in hollow core-shell nanoparticles. *Scripta Mater.* 2014;83: 1–4.
42. Krauchanka MYu, Krasnitckii SA, Gutkin MYu, Kolesnikova AL, Romanov AE. Circular loops of misfit dislocations in decahedral core-shell nanoparticles. *Scripta Mater.* 2019;167: 81–85.
43. Kolesnikova AL, Gutkin MYu, Proskura AV, Morozov NF, Romanov AE. Elastic fields of straight wedge disclinations axially piercing bodies with spherical free surfaces. *Int. J. Sol. Struct.* 2016;99: 82–96.
44. Gutkin MYu, Romanov AE. Misfit dislocations in a thin two-phase heteroepitaxial plate. *Phys. Stat. Sol. (A).* 1992;129(2): 117–126.
45. Ding Y, Sun X, Wang ZL, Sun S. Misfit dislocations in multimetallic core-shelled nanoparticles. *Appl. Phys. Lett.* 2012;100(11): 111603.
46. Gutkin MYu, Ovid'ko IA, Sheinerman AG. Misfit dislocations in wire composite solids. *J. Phys.: Condens. Matter.* 2000;12(25): 5391–5401.
47. Sheinerman AG, Gutkin MYu. Misfit dislocations in a hollow cylindrical film grown on a hole surface. *Scripta Mater.* 2001;45(1): 81–87.
48. Gryaznov VG, Heidenreich J, Kaprelov AM, Nepijko SA, Romanov AE, Urban J. Pentagonal symmetry and disclinations in small particles. *Cryst. Res. Technol.* 1999;34(9): 1091–1119.
49. Koga K, Sugawara K. Population statistics of gold nanoparticle morphologies: direct determination by HREM observations. *Surf. Sci.* 2003;529(1–2): 23–35.
50. Hofmeister H. Fivefold twinned nanoparticles. In: Nalwa HS. (ed.) *Encyclopedia of Nanoscience and Nanotechnology*. Stevenson Ranch: American Scientific Publishers; 2004. p.431–452.
51. Marks LD, Peng L. Nanoparticle shape, thermodynamics and kinetics. *J. Phys.: Condensed Matter.* 2016;28(5): 053001.
52. De Wit R. Partial disclinations. *J. Phys. C Solid State Phys.* 1972;5(5): 529–534.
53. Howie A, Marks LD. Elastic strains and the energy balance for multiply twinned particles. *Philos. Mag. A.* 1984;49(1): 95–109.
54. Krauchanka MYu, Krasnitckii SA, Gutkin MYu, Kolesnikova AL, Romanov AE, Aifantis EC. Generation of circular prismatic dislocation loops in decahedral small particles. *Scr. Mater.* 2018;146: 77–81.
55. Gutkin MYu, Kolesnikova AL, Yasnikov IS, Vikarchuk AA, Aifantis EC, Romanov AE. Fracture of hollow multiply-twinned particles under chemical etching. *Europ. J. Mech. /A Solids.* 2018;6: 133–139.
56. Khanal S, Casillas G, Bhattarai N, Velázquez-Salazar JJ, Santiago U, Ponce A, Mejía-Rosales S, José-Yacamán M. CuS_2-passivated Au-core, Au_3Cu-shell nanoparticles analyzed by atomistic-resolution Cs-corrected STEM. *Langmuir*. 2013;29(29): 9231–9239.
57. Kolesnikova AL, Gutkin MYu, Krasnitckii SA, Smirnov AM, Dorogov MV, Serebryakova VS, Romanov AE, Aifantis EC. On the elastic description of a spherical Janus particle. *Rev. Adv. Mater. Sci.* 2018;57(1/2): 246–256.

58. Petrov DA, Gutkin MYu, Kolesnikova AL, Romanov AE. Critical conditions for the formation of straight misfit dislocations in composite nanoparticles. In: *Proceedings of the 66th International Conference on Actual Problems of Strength (APP-2023), Zelenogorsk, St. Petersburg, 2023*. St. Petersburg: Izdatel'stvo VVM; 2023. p.27.
59. Petrov DA, Gutkin MYu, Kolesnikova AL, Romanov AE. Edge dislocation in an elastic sphere. *Intern. J. Eng. Sci.* 2025;210: 104226.
60. Gutkin MYu, Smirnov AM. Generation of rectangular prismatic dislocation loops in shells and cores of composite nanoparticles. *Phys. Solid State*. 2014;56(4): 731–738.
61. Gutkin MYu, Ovid'ko IA, Sheinerman AG. Misfit dislocations in composites with nano-wires. *J. Phys.: Condensed Matter*. 2003;15: 3539–3554.
62. Gutkin MYu, Krasnitckii SA, Smirnov AM, Kolesnikova AL, Romanov AE. Dislocation loops in solid and hollow semiconductor and metal nanoheterostructures. *Phys. Solid State*. 2015;57(6): 1177–1182.
63. Gutkin MYu, Smirnov AM. Initial stages of misfit stress relaxation through the formation of prismatic dislocation loops in GaN-Ga_2O_3 composite nanostructures. *Phys. Solid State*. 2016;58(8): 1611–1621.
64. Gutkin MYu, Smirnov AM. Initial stages of misfit stress relaxation in composite nanostructures through generation of rectangular prismatic dislocation loops. *Acta Mater*. 2015;88: 91–101.
65. Krasnitckii SA, Kolomoetc DR, Smirnov AM, Gutkin MYu. Misfit stress relaxation in composite core-shell nanowires with parallelepipedal cores by rectangular prismatic dislocation loops. *J. Phys.: Conf. Ser*. 2018;993: 012021.
66. Krasnitckii SA, Smirnov AM, Mynbaev KD, Zhigilei LV, Gutkin MYu. Axial misfit stress relaxation in core-shell nanowires with hexagonal core via nucleation of rectangular prismatic dislocation loops. *Materials Physics and Mechanics*. 2019;42(6): 776–783.
67. Krasnitckii SA, Smirnov AM, Gutkin MYu. Axial misfit stress relaxation in core-shell nanowires with polyhedral cores through the nucleation of misfit prismatic dislocation loops. *J. Mater. Sci*. 2020;55: 9198–9210.
68. Gutkin MYu, Mordasova EA, Kolesnikova AL, Romanov AE. Misfit stress relaxation at boundaries of finite-length tubular inclusions through the generation of prismatic dislocation loops. In: Altenbach H, Bruno G, Eremeyev VA, Gutkin MYu, Müller WH. (eds.) *Mechanics of Heterogeneous Materials. Advanced Structured Materials*. Cham: Springer; 2023. p.139–157.
69. Gutkin MYu, Kolesnikova AL, Krasnitckii SA, Mikaelyan KN, Mikheev DS, Petrov DA, Romanov AE, Smirnov AM, Chernakov AP. Dislocation mechanisms of misfit stress relaxation in crystalline nanoheterostructures. *Phys. Met. Metallogr*. 2024;125(1): 1211–1218.
70. Raychaudhuri S, Yu ET. Critical dimensions in coherently strained coaxial nanowire heterostructures. *J. Appl. Phys*. 2006;99(11): 114308.
71. Zhao YX, Fang QH, Liu YW. Edge misfit dislocations in core–shell nanowire with surface/ interface effects and different elastic constants. *Int. J. Mech. Sci*. 2013;74: 173–184.
72. Enzevaee C, Gutkin MYu, Shodja HM. Surface/interface effects on the formation of misfit dislocation in a core–shell nanowire. *Philos. Mag*. 2014;94(5): 492–519.
73. Wang X, Pan E, Chung PW. Misfit dislocation dipoles in wire composite solids. *Int. J. Plast*. 2010;26(9): 1415–1420.
74. Arjmand M, Benjamin C, Szlufarska I. Analytical elastoplastic analysis of heteroepitaxial core-shell nanowires. *AIP Advances*. 2019;9(5): 055119.
75. Ovid'ko IA, Sheinerman AG. Misfit dislocation loops in composite nanowires. *Philos. Mag*. 2004;84(20): 2103–2118.
76. Aifantis KE, Kolesnikova AL, Romanov AE. Nucleation of misfit dislocations and plastic deformation in core/shell nanowires. *Philos. Mag*. 2007;87(30): 4731–4757.
77. Colin J. Prismatic dislocation loops in strained core-shell nanowire heterostructures. *Phys. Rev. B*. 2010;82(5): 054118.
78. Haapamaki CM, Baugh J, LaPierre RR. Critical shell thickness for InAs-$Al_xIn_{1-x}As$(P) core-shell nanowires. *J. Appl. Phys*. 2012;112(12): 124305.
79. Salehzadeh O, Kavanagh KL, Watkins SP. Geometric limits of coherent III-V core/shell nanowires. *J. Appl. Phys*. 2013;114(5): 054301.
80. Colin J. Circular dislocation loop in a three-layer nanowire. *Int. J. Solids Struct*. 2015;63: 114–120.
81. Chu HJ, Wang J, Zhou CZ, Beyerlein IJ. *Self*-energy of elliptical dislocation loops in anisotropic crystals and its application for defect-free core/shell nanowires. *Acta Mater*. 2011;59(18): 7114–7124.
82. Smirnov AM, Krasnitckii SA, Gutkin MYu. Generation of misfit dislocations in a core-shell nanowire near the edge of prismatic core. *Acta Mater*. 2020;186: 494–510.
83. Fang QH, Chen JH, Wen PH, Liu YW. Misfit dislocations in an annular strained film grown on a cylindrical nanopore surface. *Scr. Mater*. 2009;60(6): 395–398.

84. Zhao YX, Fang QH, Liu YW. Edge misfit dislocation formation at the interface of a nanopore and infinite substrate with surface/interface effects. *Philos. Mag.* 2012;92(34): 4230–4249.
85. Ertekin E, Greaney PA, Chrzan DC, Sands TD. Equilibrium limits of coherency in strained nanowire heterostructures. *J. Appl. Phys.* 2005;97(11): 114325.
86. Glas F. Critical dimensions for the plastic relaxation of strained axial heterostructures in free-standing nanowires. *Phys. Rev. B*. 2006;74(12): 121302.
87. Ye H, Yu Z. Plastic relaxation of mixed dislocation in axial nanowire heterostructures using Peach-Koehler approach. *Phys. Stat. Sol. RRL*. 2014;8(5): 445–448.
88. Kolesnikova AL, Chernakov AP, Gutkin MYu, Romanov AE. Misfit strain induced out-of-interface prismatic dislocation loops in axially inhomogeneous hybrid nanowires. *Extr. Mech. Lett.* 2022;56(10): 101861.
89. Nabarro FRN. The force between misfit dislocations. *Philos. Mag.* 1970;22(178): 803–808.
90. Ovid'ko IA, Sheinerman AG. Perfect, partial, and split dislocations in quantum dots. *Phys. Rev. B*. 2002;66(24): 245309.
91. Petrov DA, Gutkin MYu. Critical conditions of misfit dislocation formation in a bilayer cylinder. In: Zaytsev DV. (ed.) *Abstracts of the LXVII International Conference "Advanced Problems of Strength" (April 2–5, 2024, Yekaterinburg, Russia)*. Yekaterinburg: Izd-vo UGGU; 2024. p.70–72. (In Russian)
92. Petrov DA, Gutkin MYu. Longitudinal misfit dislocations in a bilayer nanowire. In: Straumal BB. (ed.) *Physics of Condensed Matter: Abstracts of the IV International Conference (June 2-6, 2025, Chernogolovka, Russia)*. Chernogolovka; 2025. p.144. (In Russian)
93. Petrov DA, Gutkin MYu. Critical conditions for the formation of longitudinal and transverse misfit dislocations in a symmetrical bilayer cylinder. In: Yurlova NA. (ed.) *XXIV Winter School on Continuum Mechanics (February 24-28, 2025, Perm', Russia). Book of Abstracts*. Perm: Izd-vo ICMM UB RAS; 2025. p.220. (In Russian)
94. Bonnet R. Elasticity theory of straight dislocations in a multilayer. *Phys. Rev. B*. 1996;53(16): 10978–10982.
95. Bonnet R. A thin bicrystal deformed by a two period network of misfit dislocations. *Compt. Rend. Acad. Sci., Ser. II*. 1999;327(13): 1331–1336.
96. Zhang TY, Lee S, Guido LJ, Hsueh CH. Criteria for formation of interface dislocations in a finite thickness epilayer deposited on a substrate. *J. Appl. Phys.* 1999;85(11): 7579–7586.
97. Bonnet R. A biperiodic network of misfit dislocations in a thin bicrystalline foil. *Phys. Stat. Sol. A*. 2000;180(2): 487–497.
98. Wang SD. Energy of an array of dislocations in a strained epitaxial layer deposited on a finite substrate. *J. Appl. Phys.* 2000;88(12): 7089–7094.
99. Outtas T, Adami L, Derardja A, Madani S, Bonnet R. Anisotropic elastic field of a thin bicrystal deformed by a biperiodic network of misfit dislocations. *Phys. Stat. Sol. A*. 2001;188(3): 1041–1045.
100. Outtas T, Adamia L, Bonnet R. A biperiodic interfacial pattern of misfit dislocation interacting with both free surfaces of a thin bicrystalline sandwich. *Solid State Sciences*. 2002;4(2): 161–166.
101. Vattré A. Mechanical interactions between semicoherent heterophase interfaces and free surfaces in crystalline bilayers. *Acta Mater.* 2015;93: 46–59.
102. Vattré A. Elastic interactions between interface dislocations and internal stresses in finite-thickness nanolayered materials. *Acta Mater.* 2016;114: 184–197.
103. Colin J. Dislocation climbing in a three-layer structure. *Acta Mech.* 2024; 235: 5661–5672.
104. Neily S, Ghabri H, Youssef S, Bonnet R. Screw heterointerfacial dislocations piercing a thin plate. *Comptes Rendus Physique.* 2018;19(5): 341–346.
105. Ghabri H, Neily S, Youssef S, Bonnet R. Screw misfit dislocations perpendicular to one or two free surfaces. *Philos. Mag. Lett.* 2018;98(6): 227–239.
106. Colin J. Misfit dislocation formation in stressed nanofilms. *Philos. Mag. Lett.* 2014;94(4): 189–197.
107. Colin J. Equilibrium positions of misfit dislocations in a nanolayer embedded in a matrix. *Intern. J. Sol. Struct.* 2016;81: 393–398.
108. Colin J. Formation of a prismatic dislocation loop in the interface of a circular cylindrical inclusion embedded in a thin slab. *J. Appl. Mech.* 2016;83(2): 021006.
109. Mikaelyan KN, Gutkin MYu, Borodin EN, Romanov AE. Dislocation emission from the edge of a misfitting nanowire embedded in a free-standing nanolayer. *Intern. J. Sol. Struct.* 2019;161: 127–135.
110. Malyshev KL, Gutkin MYu, Romanov AE, Sitnikova AA, Sorokin LM. *Dislocation models and diffraction contrast of rod-like defects in silicon. Preprint No.1109*. Leningrad: A.F. Ioffe Physico-Technical Institute; 1987. (In Russian).
111. Gutkin MYu, Romanov AE. Straight edge dislocations in a thin two-phase plate. I. Elastic stress fields. *Phys. Stat. Sol. A*. 1991;125(1): 107–125.
112. Gutkin MYu. Elastic behavior of defects in nanomaterials. I. Models for infinite and semi-infinite media. *Rev. Adv. Mater. Sci.* 2006;13(2): 125–161.